

## BARFORM DEPOSITS OF THE CAROLYN SHOEMAKER FORMATION, GALE CRATER, MARS

BENJAMIN T. CARDENAS,\*<sup>1</sup> JOHN P. GROTZINGER,<sup>1</sup> MICHAEL P. LAMB,<sup>1</sup> KEVIN W. LEWIS,<sup>2</sup> CHRISTOPHER M. FEDO,<sup>3</sup> ALEXANDER B. BRYK,<sup>4</sup> WILLIAM E. DIETRICH,<sup>4</sup> NATHAN STEIN,<sup>1</sup> MADISON TURNER,<sup>2</sup> AND GWÉNAËL CARAVACA<sup>5</sup>

<sup>1</sup>*Division of Geological and Planetary Sciences, California Institute of Technology, Pasadena, California 91125, U.S.A.*

<sup>2</sup>*Department of Earth and Planetary Sciences, Johns Hopkins University, Baltimore, Maryland 21218, U.S.A.*

<sup>3</sup>*Department of Earth and Planetary Sciences, The University of Tennessee Knoxville, Knoxville, Tennessee 37996, U.S.A.*

<sup>4</sup>*Department of Earth and Planetary Science, University of California, Berkeley, California 94720, U.S.A.*

<sup>5</sup>*UMR 5277 CNRS, UPS, CNES Institut de Recherche en Astrophysique et Planétologie, Université Paul Sabatier Toulouse III, Toulouse, France  
e-mail bcardenas@psu.edu*

**ABSTRACT:** The early environmental history of Mars is encoded in the planet's record of sedimentary rocks. Since 2012, the Curiosity rover has been ascending Mount Sharp, Gale crater's central mound, making detailed observations of sedimentary strata exposed there. The primary depositional setting represented by the rocks examined thus far has been a perennial lake, represented by the mudstones and sandstone lenses of the Murray formation. Here, we report on the sedimentology of outcrops examined in the Carolyn Shoemaker formation, which sits stratigraphically above the Murray formation. We interpret strata exposed in the Glasgow and Mercou members of the Carolyn Shoemaker formation to represent river bars in ancient alluvial and shoreline settings based on sedimentary structures, stratal geometries measured from photogrammetric data, and erosional morphology. The transition from a lacustrine to a fluvial depositional setting records the aggradation and progradation of coastal rivers into what was previously the extent of the Gale lake system. This may have occurred due to the shrinking of the lake over time due to climate-driven changes in the basin water balance, or local three-dimensionality in shoreline evolution, such as the formation of a new sedimentary lobe following a channel switch.

### INTRODUCTION

The history of water on the surface of Mars is encoded into the planet's sedimentary rocks (Grotzinger and Milliken 2012). Since 2012, the Mars Science Laboratory (MSL) mission's Curiosity rover has provided the means for field-scale investigations of sedimentary rocks in Gale crater, a 155-km-wide impact crater near the martian equator, which is proposed to have held a lake during the Noachian–Hesperian transition about 3.6 Ga, a time when water flowed freely across both hemispheres of the martian surface (Fig. 1A, B; e.g., Gulick 2001; Fassett and Head 2008; Burr et al. 2009; Dickson et al. 2020). Sedimentology has been pivotal for understanding ancient depositional settings recorded across Gale crater, which includes shorelines (Grotzinger et al. 2014, 2015), lakes (Grotzinger et al. 2014; Stack et al. 2019), rivers (Williams et al. 2013a; Szabó et al. 2015; Edgar et al. 2017), and sand seas (Banham et al. 2018, 2021; Bedford et al. 2020). Sedimentological studies have provided not only broadly defined depositional settings, but also important details about these settings including lake salinity (Stack et al. 2019), lake-drying episodes (Stein et al. 2018), wind regimes (Banham et al. 2018, 2021; Bedford et al. 2020), sediment transport (Szabó et al. 2015; Edgar et al. 2017), sediment sources (Edgett et al. 2020), and the role of waves and presence/absence of ice cover (Rubin et al. 2022), all of which help further constrain the evolution of the ancient martian surface at a time when it may have been

habitable. Indeed, the history recorded in the stratigraphy at Gale crater is one that describes a potentially habitable environment throughout the deposition of the Murray formation.

The Carolyn Shoemaker formation, located stratigraphically above the Murray formation, records a significant shift in depositional setting, broadly recorded by an increase in the sandstone-to-mudstone ratio (Caravaca et al. 2022) (Fig. 1C). Here, we present results regarding the depositional setting of this formation, and what it might represent for the evolution of Gale's ancient habitable environments. We examined two exposures of sedimentary rock in Gale crater investigated between mission sols (Mars days) 2,943 and 3,083 in the Glasgow and Mercou members of the Carolyn Shoemaker formation (Fig. 1). Mont Mercou, one of two high-standing ridges located at the transition to the cross-bedded facies that define the Mercou member, and the bench-forming exposures of the Glasgow member are located 1.2 km apart laterally and 30 m apart vertically (Fig. 2). We use sedimentary structures, bed orientations, and paleotransport measurements to interpret the depositional setting at these locations as alluvial. That is, these strata were deposited by net-depositional rivers that created their own beds of sediment, rather than net-erosional rivers incising into bedrock.

Alluvial rivers were commonplace across the surface of Mars during the Noachian–Hesperian transition, particularly around the boundary between the topographically high southern hemisphere and the low northern hemisphere where Gale crater is located (Burr et al. 2009, 2010; DiBiase et al. 2013; Williams et al. 2013a; Kite et al. 2015; Davis et al. 2016, 2019; Cardenas et al. 2018; Hughes et al. 2019; Balme et al. 2020; Dickson et al.

\*Present Address: Department of Geosciences, The Pennsylvania State University, University Park, Pennsylvania 16802, U.S.A.

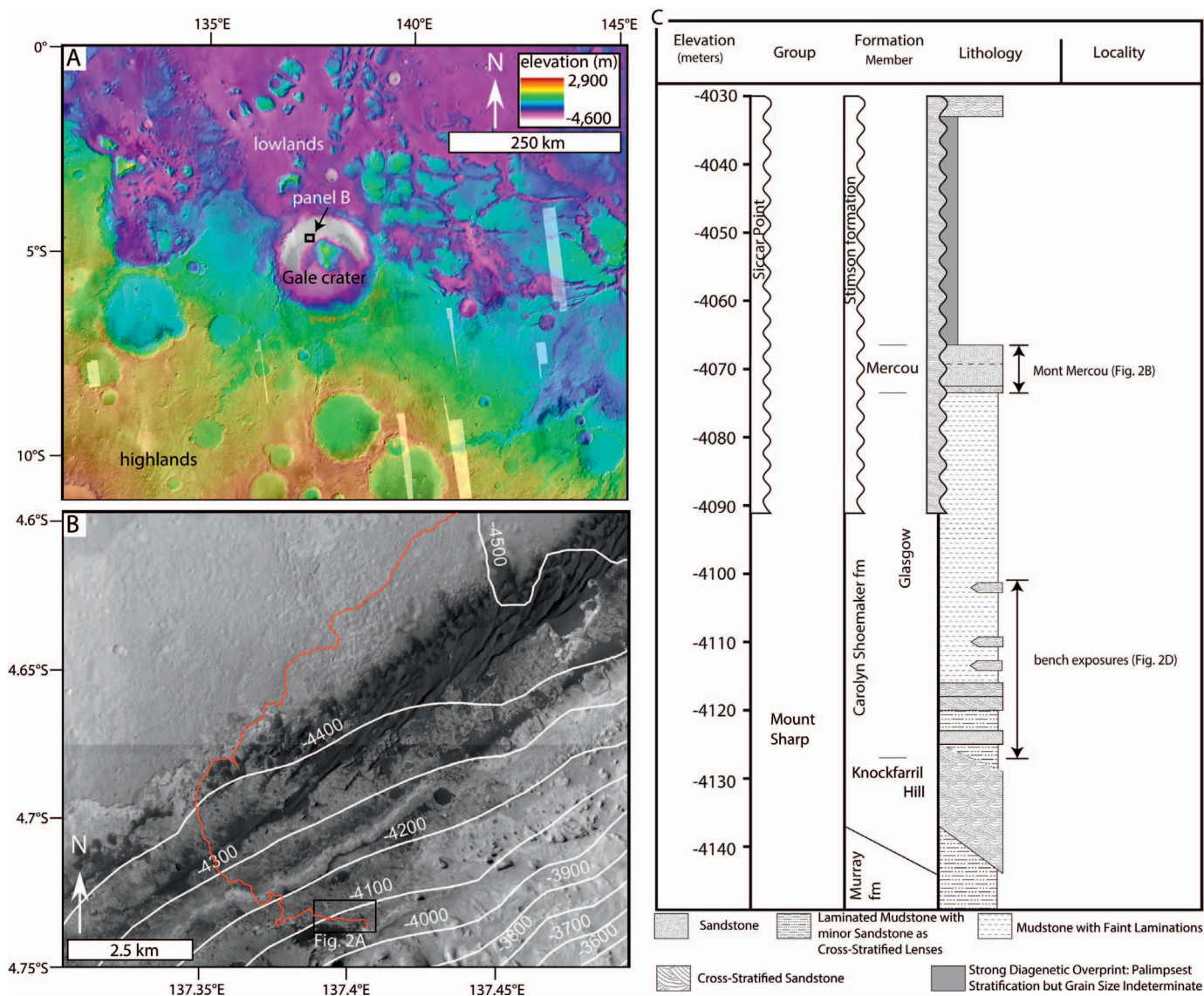


FIG. 1.—Geographic and stratigraphic context. **A**) Digital elevation model showing Gale crater's location along the planet's highlands–lowlands boundary. The location of Part B is shown in the black box. **B**) Zoom in to the rover traverse from north to south (red line). Contours are at 100 m intervals. The location of the study area shown in Figure 2A is shown. **C**) Gale crater's stratigraphic column showing the intervals of the Carolyn Shoemaker formation studied here.

2020). These alluvial sequences can be identified where they form ridges observed in orbiter image data due to the differential erosion of coarse-grained channel belts and fine-grained overbank deposits (Pain et al. 2007; Williams et al. 2007; DiBiase et al. 2013; Hayden et al. 2019; Cardenas et al. 2020; Hayden and Lamb 2020; Clarke et al. 2020). Thus far, Curiosity's observations of the Carolyn Shoemaker formation, as well as lower parts of the Murray and Yellowknife Bay formations (Williams et al. 2013a; Edgar et al. 2017), provide the opportunity to examine alluvial strata in detail to complement orbiter-based observations.

#### METHODS

The objective of our study is to understand the depositional settings of the selected outcrops using geometric measurements of the sedimentary structures exposed there, as well as measurements and observations of the erosional geomorphology of the outcrops. We focus our analyses on Mastcam (Malin et al. 2017) data collected during two imaging campaigns.

The Mastcam instrument on Curiosity consists of two fixed-focal-length cameras (34 mm and 100 mm) mounted on the rover mast at a height of approximately 2 meters. The cameras are separated by a distance of 24.64 cm, with a toe-in of 2.5 degrees to allow stereo imaging.

#### Imaging Campaigns

The imaging campaign at Mont Mercou was focused on moving into two close positions to the cliff face in order to perform high-resolution stereo imaging using both Mastcams at three locations. A close approach was made at an eastern location, and another at the western edge of the north-facing cliff face. The image IDs used for stereo measurements are shown in Table 1. Following the close approaches, the rover continued around and up the western flank of Mont Mercou (Fig. 2).

Imaging of the Glasgow member exposures was primarily performed during the ascent from the Mary Anning drill location (Fig. 2). A close approach was made to the outcrop Maybole, followed by a path selected as

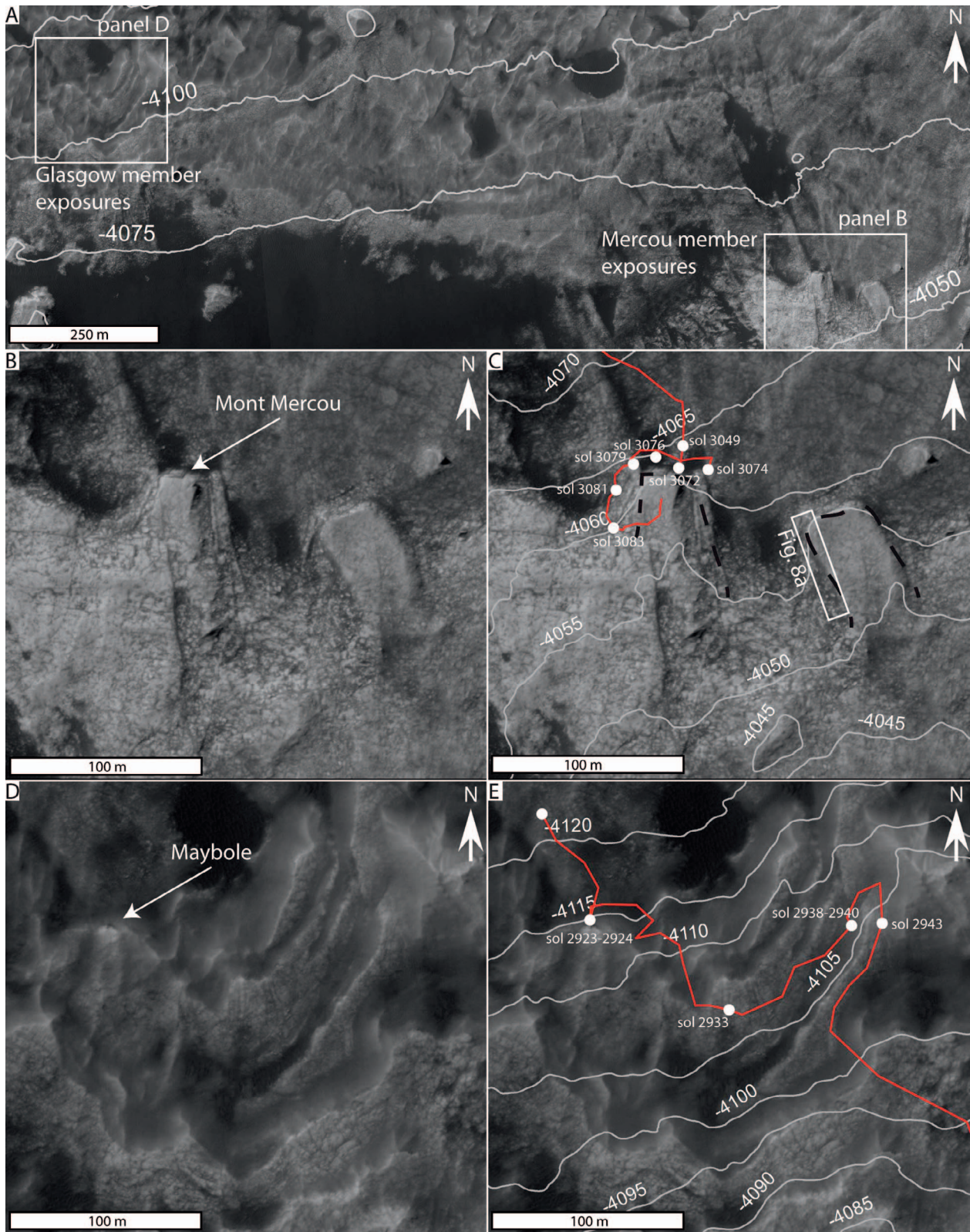


FIG. 2.—Location maps of the two study areas at Gale crater, Mars. Sol (Mars day) locations can be used to locate images throughout the manuscript. **A)** HiRISE image of the region containing the two exposures studied here. Topographic contours at 25 m intervals are overlain. Boxes show the locations of the two exposures. **B)** Zoom in to the Mont Mercou ridge on the left, and the unapproached ridge on the right. **C)** Same as Part B with 5 m contours in white and Curiosity's traverse around the north and west sides, and finally along the top of the ridge, shown in red. Stops are shown at white dots with the mission sol adjacent. Mont Mercou and the adjacent unapproached ridge are outlined with a dashed black line. **D)** Zoom in to the curved bench-forming Glasgow member exposures. An arrow points to the Maybole outcrop. **E)** Same image as Part D, with the same contour intervals and traverse notation as in Part D.

TABLE 1.—Statistics on dip directions and magnitudes measured from stereo Mastcam data. The number of individual measurements is shown by the *n* value. *P*-values represent the similarity of the original results, which are presented here, and the Monte Carlo simulated results. All comparisons are unable to reject the similarity of the datasets.

Location	image sequence	n	Dip Directions			Dip Magnitudes		
			mean	sigma	p-value	mean	sigma	p-value
Mont Mercou, central	mcam16055 sol 3074	290	321°	33°	0.99	8°	4°	1
Mont Mercou, western end	mcam16076 sol 3079	353	327°	61°	1	12°	7°	1
Mont Mercou, eastern end	mcam16054 sol 3074	315	107°	64°	0.99	19°	9°	1
Glasgow, Maybole	mcam15267 sol 2926	535	276°	11°	0.42	21°	7°	0.99
Glasgow, central	mcam15328 sol 2983	120	122°	38°	0.94	4°	8°	0.08
Glasgow, eastern end	mcam15342 sol 2940	211	356°	35°	0.94	8°	4°	0.99

a combination of lowest slopes and best imaging opportunities. Given the area of exposures, stereo data were collected strategically, with more extensive coverage from the lower-resolution Mastcam 34 mm camera. The stereo images used here are also shown in Table 1.

In an effort to measure grain size (Edgett et al. 2012), Mars Hand Lens Imager (MAHLI) images were collected at the Glasgow exposures. However, no clear measurements could be made. A MAHLI malfunction precluded imaging of the Mercou member.

#### Mastcam Mosaics

We acquired individual Mastcam 34 mm and 100 mm frames from the publicly accessible Cartography and Imaging Sciences Planetary Data System Node (PDS; <https://pds-imaging.jpl.nasa.gov/volumes/msl.html>). We converted the raw data format, .IMG, into .PNG, and used the automatic stitch function in Adobe Photoshop to create mosaics for line sketches. Mastcam image sequences are listed in the figure captions.

#### Stereo Measurements

Stereo digital elevation models were derived from Mastcam image data products using a pipeline similar to that described by Deen and Lorre (2005) and Alexander et al. (2006), using JPL's VICAR software package (<https://github.com/NASA-AMMOS/VICAR>). Raw Mastcam images are demosaicked to interpolate over the Bayer color grid using the algorithm of Malvar et al. (2004). Demosaicked images are decompanded (converted back from 8 to 12 bit using a lookup table), radiometrically corrected, and linearized (projected to a linear CAHV camera model, Yakimovsky and Cunningham (1978)). Linearization results in epipolar-aligned and equally scaled images, from which a 1-D correlation is conducted across the image pair. The resulting 1-D disparity maps are then unprojected to the original image space, and a 2-D correlation is performed on the original (unlinearized, but demosaicked and radiometrically corrected) images. This 2-D matching process generally improves the image correlation over the initial 1-D process. Finally, the resulting 2-D disparity map is transformed to a DTM in site-frame coordinates using the known camera position and orientation.

We used three products associated with a Mastcam stereo frame to measure the local orientation of stratigraphic surfaces: a visible image used for mapping, a three-band raster containing XYZ data, and a three-band raster containing the associated error in XYZ. In a Geographic Information System (GIS) Mastcam visible stereo frames were placed on top of Mastcam stereo XYZ and XYZ-error rasters. We mapped bedding planes on vertical exposures as polyline shapefiles in the GIS and converted polylines to a series of points. At those points, we extracted XYZ and XYZ-error data from the co-located stereo rasters. Mapping on these stereo frames is limited to a single frame at a time to avoid distortion associated with mosaicking. Many of the Mastcam mosaics shown here consist of several dozen or for some over 100 individual frames, each imaging a few

cm to a few tens of centimeters of outcrop. As such, the lines we mapped and fit planes to during this process ranged from a few centimeters to a few tens of centimeters. Because of this, the measurements presented here represent the full three dimensionality of these strata sampled over several meters, rather than spatial averages over several meters.

Using the Python application Attitude (Quinn and Ehlmann 2019), we found the dip magnitude and direction of the best-fit plane for each bounding surface. Using the XYZ-error values for each point along every mapped bounding surface, we performed 1,000 Monte Carlo simulations to find the orientation of other possible plane fits within the given error of each point along a bounding surface (Stein et al. 2020). We plotted the distribution of these simulated planes on rose diagrams and identified poorly fit planes with bimodal or diffuse solutions, which composed only a small percentage of the measurements. For each set of measurements from a particular location, we statistically tested the similarity of the orientations of measured planes with all orientations produced during the Monte Carlo simulations. Poorly fitted planes would produce a wide array of Monte Carlo solutions and thus dissimilar distributions. We compared dip magnitudes to the Monte Carlo results using a two-sample Kolmogorov-Smirnov test. To compare dip directions, we used two-sample Kuiper tests, which are designed to test the similarity of circular datasets. Means and standard deviations in dip-direction data were calculated using the CircStat toolbox in Python (Berens 2009). To provide context for these measurements, we completed outcrop sketches on Mastcam mosaics. To support rover observations, we used HiRISE image PSP\_009149\_1750 and a stereo-pair elevation model generated from this image and PSP\_009294\_1750, which we used to calculate contours for Figure 2 and to generate slope maps using GIS toolboxes. The Context Camera seamless global mosaic (Dickson et al. 2020) and Mars Orbiting Laser Altimeter (Smith et al. 2001) data were used to create Figure 1B and C. For additional visualization, we created 3D outcrop models of the Mont Mercou and Maybole outcrops (see Appendix for details and a link).

## RESULTS

Dip directions and magnitudes presented here, and shown in detail in Table 1, all have statistically significant similarity to their Monte Carlo simulated distributions, indicating a high level of confidence in the measurements. This is particularly true for the measurements made from the close-approach images to Mont Mercou. Importantly, all measurements match general trends observed by eye in the mosaics.

#### Mercou Member

Though the Glasgow member exposures were observed by the rover before the Mercou member, we are presenting Mont Mercou first, as it is well exposed in three dimensions that proved useful for understanding the less-well exposed Glasgow member strata. Mont Mercou stands 6.78 m tall (Fig. 3) along a nearly vertical cliff face 21 m wide (aspect ratio of 3.1) that

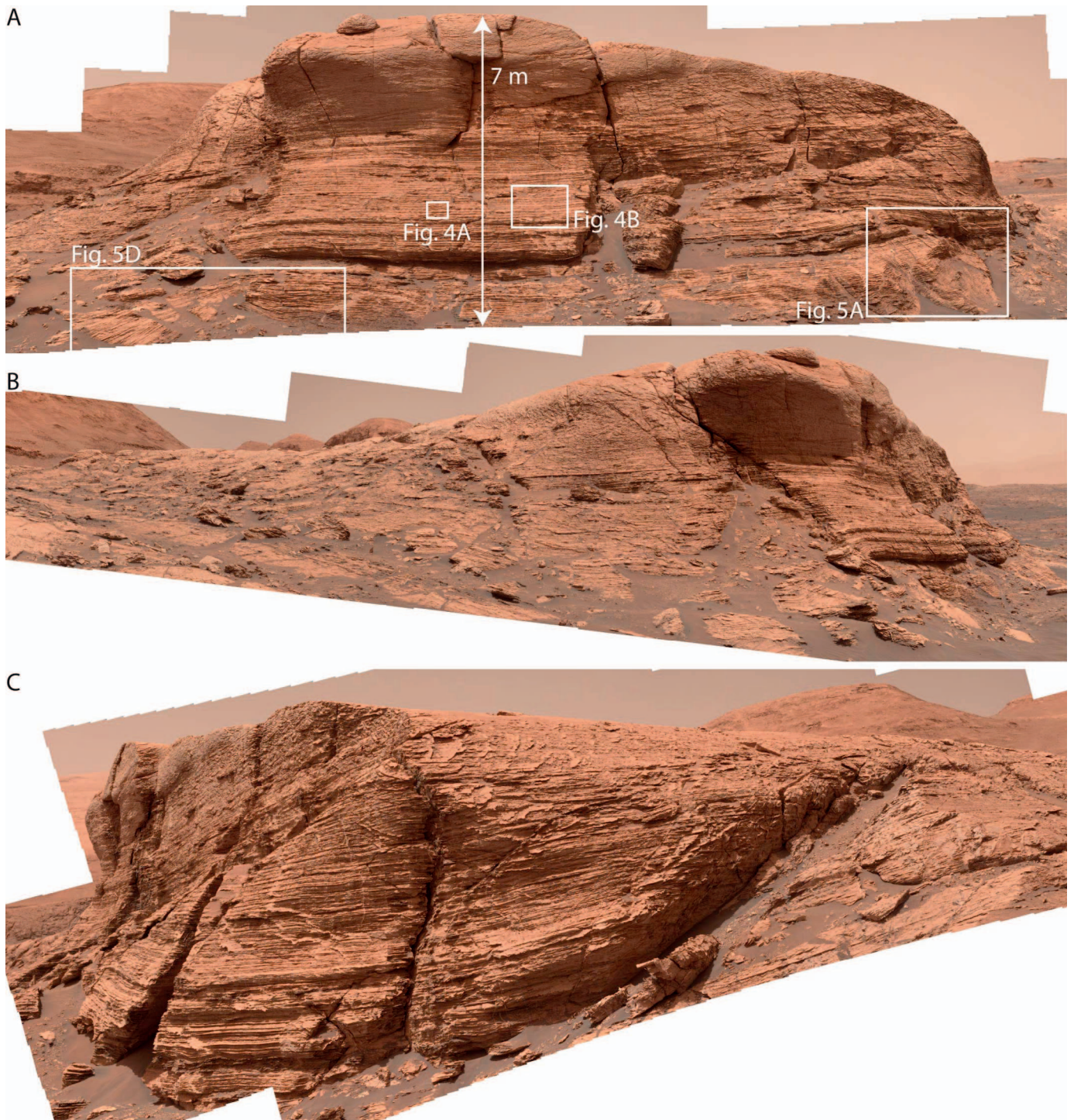


FIG. 3.—**A**) The north-facing cliff face of Mont Mercou (mcam15933, mission sol 3051, looking south). Boxes show the locations of other figures taken during close approaches. **B**) The eastern flank of Mont Mercou (mcam16061, mission sol 3076, looking southwest). **C**) The western flank of Mont Mercou (mcam16090, mission sol 3081, looking southeast) (Mastcam image credit: NASA/Caltech-JPL/MSSS).

trends east–west at the end of a 100-m-long north–south-trending ridge (Fig. 2). The upper 2.80 m (41%) appears to be structureless, likely due to diagenetic modification (Seeger et al. 2021), and will not be discussed further here. The bottom 3.98 m (59% of the thickness) is composed of well-defined sedimentary structures. The most prominent sedimentary structures of Mont Mercou are the planar beds and laminae observed

across the cliff face, composing a section 3.34 m thick (49% of the total thickness) (Fig. 4A). Though there is continuity in these beds at the meter scale, we identified a limited section of offset beds (Fig. 4B). The offset appears to drop to zero beneath the structureless region of the cliff face. In the central image, these beds dip towards the northwest with a mean dip of

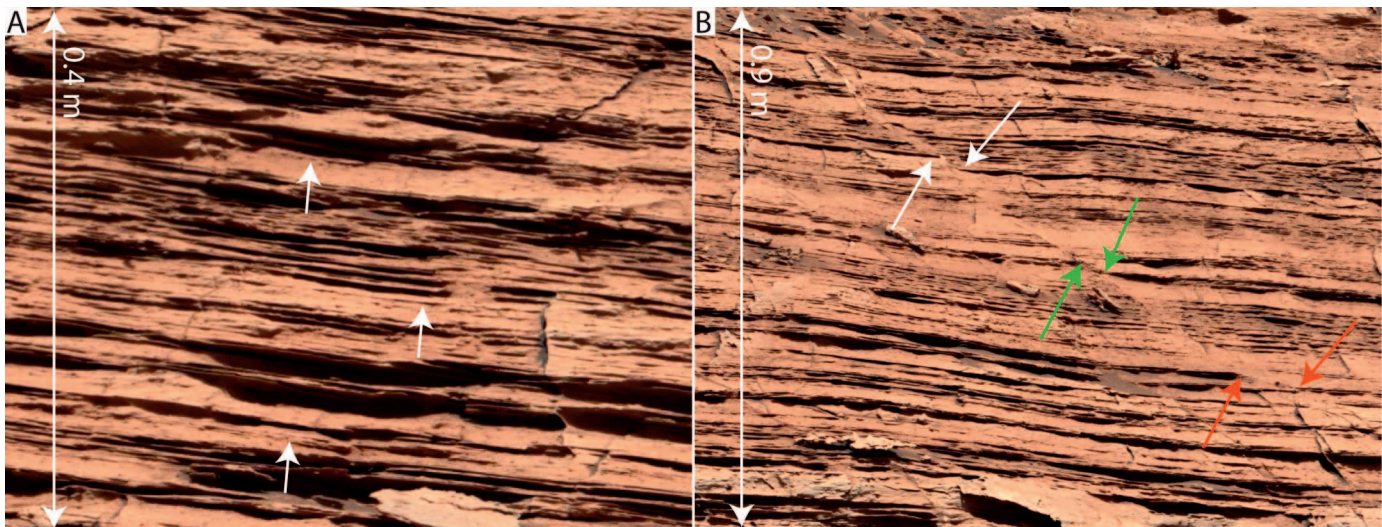


Fig. 4.—Characteristic bedding of the Mont Mercou cliff face (meam16055, mission sol 3074, looking south). **A)** Planar beds of the Mont Mercou cliff face (location shown in Fig. 3A). White arrows point to locations where bedding can be observed in units that elsewhere appear structureless. **B)** Offset strata (location shown in Fig. 3A). Colored arrows point to beds with similar erosional expressions on either side of a small growth fault, with offset increasing down the fault (Mastcam image credit: NASA/Caltech-JPL/MSSS).

8° (Table 1). Across the exposure, adjacent beds are variably recessive enough to be identified by shadowing (e.g., Fig. 4).

At the western end of the cliff face, bed orientations change across a scour surface, dipping towards the west with a mean dip of 12° (Table 1). Modes near 270° represent strata on the western end of the scour, while modes near 300° and 000° represent strata on the eastern side of the scour and draped above the scour (Figs. 5A–C, 6). The scour surface persists to a height of 0.64 m above the base of the exposure, but bedding orientations change above that in a draping pattern, with a visible and gradual decrease in the reorientation upsection (Fig. 5). A similar change in bedding orientation is observed at the eastern end of the outcrop 13 m away (Figs. 5D–H, 6). There, beds reorient towards an eastern dip direction with a mean dip of 19° (Table 1), though we could not confirm if a similar scour surface exists here due to sand cover. Sedimentary structures do not change in concert with either of these changes in bed orientation (Fig. 5). Together, the measured changes in dip direction reflect a 13-m-wide north-convex structure.

The bottom 0.64 m of Mont Mercou contains trough cross strata in nearly vertical exposures (Fig. 5). On the western flank of Mont Mercou, trough cross strata are exposed along surfaces dipping 10–20°, similar to the dips of the planar beds (Fig. 6). In these outcrops, bounding surfaces package strata with a clear southward concavity that we interpreted as planview dune-trough cross strata, and used as an indicator of paleotransport direction (Fig. 7).

A similar ridge east of Mont Mercou was not approached, but observations made from Mont Mercou about 100 m away show similar inclined strata in coherent exposures that appear to be in place (Figs. 2, 8).

### *Glasgow Member*

The topographic benches (elongated flat surfaces bound by steeply dipping surfaces; Fig. 9) exposing the Glasgow member span 16 m in elevation (Fig. 2). Curiosity traversed five successive benches from bottom to top, each bench 2 to 4 m higher than the previous. Bench tops have a median slope of 5° with a standard deviation of 3° towards, away, and along bench tops. Slopes between benches have a median slope of 17° with a standard deviation of 6°, and are as steep as 30°. The curved planview geometry of the benches forms a convex-south shape (Fig. 2). Most of the

exposures of the Glasgow member occur along bench margins and tops, which are observable from both rover- and orbiter-based remote sensing data (Fig. 2). Strata are not clearly exposed along the hillslopes located between benches (Fig. 9). The bench margins themselves can be either rounded or cliff forming, and some bench strata form an overhang above the hillslope below (Fig. 9). Together, these form a scarp-and-slope morphology (Fig. 9). Some outcrops exposed along topographic benches in the Glasgow member of the Carolyn Shoemaker formation have many of the same sedimentary structures observed at Mont Mercou. Most exposures feature planar beds and laminae with low-angle truncations, non-parallel strata, and variably recessive beds (Fig. 10). Bedding at the Maybole outcrop (Fig. 11), the topographically lowest exposure, dips on average 21° towards the west (Table 1). The dip directions of planar beds measured along the tops of benches changes from southeast with a mean dip of 14° at a central location, to north along the snout of a bench with a mean dip of 8°. Together, these measurements represent a 125-m-wide south-convex structure. At the locations where we were able to measure, these dip directions change in concert with the geomorphic curves of the exposed bench tops, such that the stratigraphic dip directions dip away from bench edges (Fig. 12), suggesting that bench morphology is related to the geometry of the deposit.

### DISCUSSION

Regionally, stratal orientations in Gale crater measured from the rover are within a few degrees of flat lying (Stein et al. 2020), with no suggestion of major postdepositional terrain movement. We therefore infer that all dip directions and dip magnitudes presented below are primary and reflect the original orientation of stratal surfaces.

### *Mercou Member Interpretation*

Several hypothesized depositional settings of the strata at Mont Mercou can be tested using the combination of facies, dip directions, and paleotransport directions we collected (Fig. 13). The back and front of a downstream-migrating fluvial bar or deltaic mouth bar are both consistent with a convex arrangement of dip directions. The fronts and backs of these bars can be distinguished from each other using the relative direction of

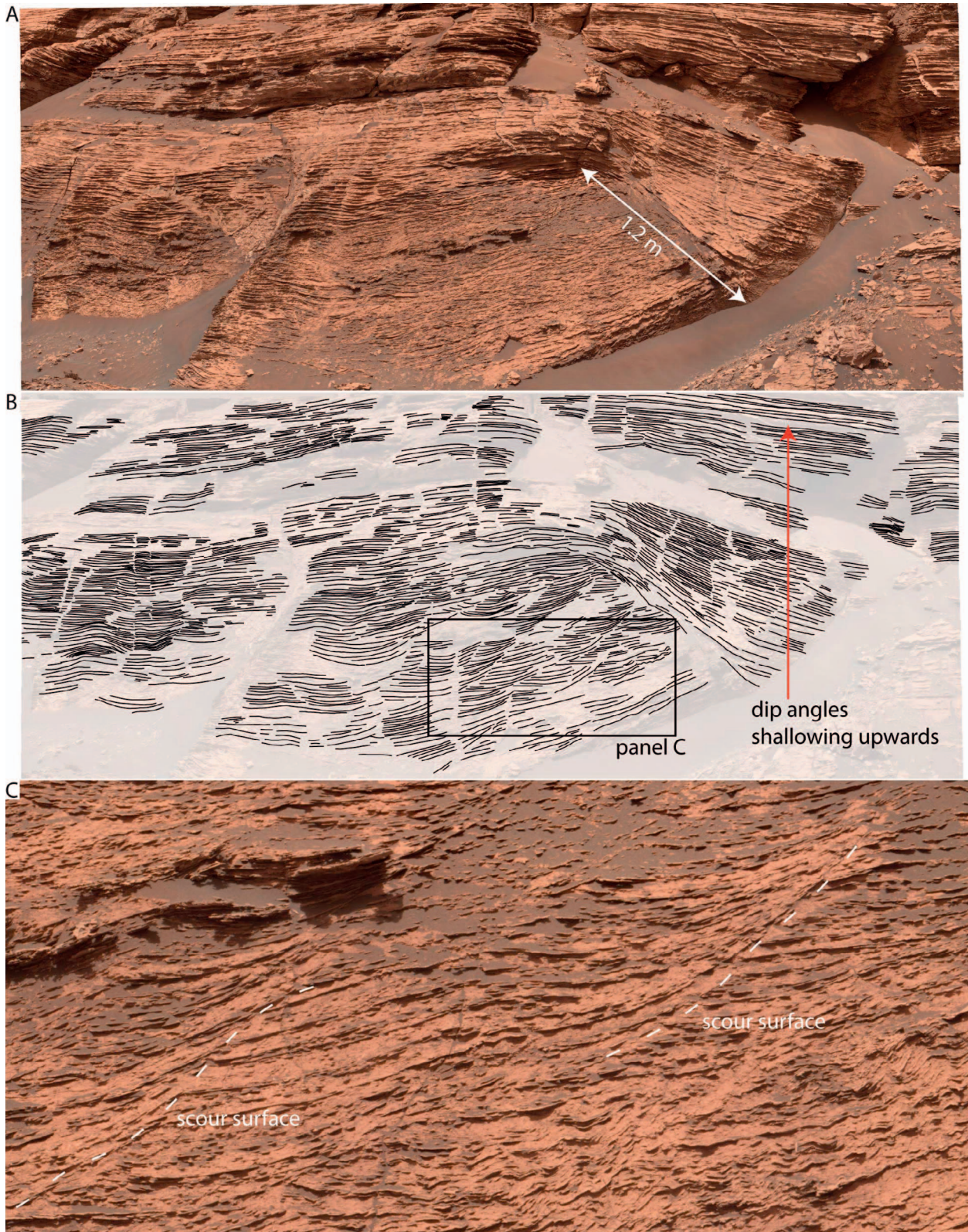


FIG. 5.—**A**) Eastern scour of Mont Mercou (mcam16054, mission sol 3074, looking south). **B**) Interpretation, with boxes showing the location of Part C. Red arrow shows the draping strata above the scour decreasing in dip upwards. **C**) Dune trough cross strata, with white dashed lines marking scour surfaces at set boundaries. **D**) Western scour of Mont Mercou (mcam16076, mission sol 3079). **E**) Interpretation of Part D showing the locations of Parts F and G. **F**) Superimposed ripple cross laminations on larger-scale dipping strata. The blue arrow shows inferred transport direction from the ripple cross laminations. **G**) Compound ripple and dune cross bedding. The blue arrow shows the inferred paleotransport direction from the dune-scale cross bedding (Mastcam image credit: NASA/Caltech-JPL/MSSS).

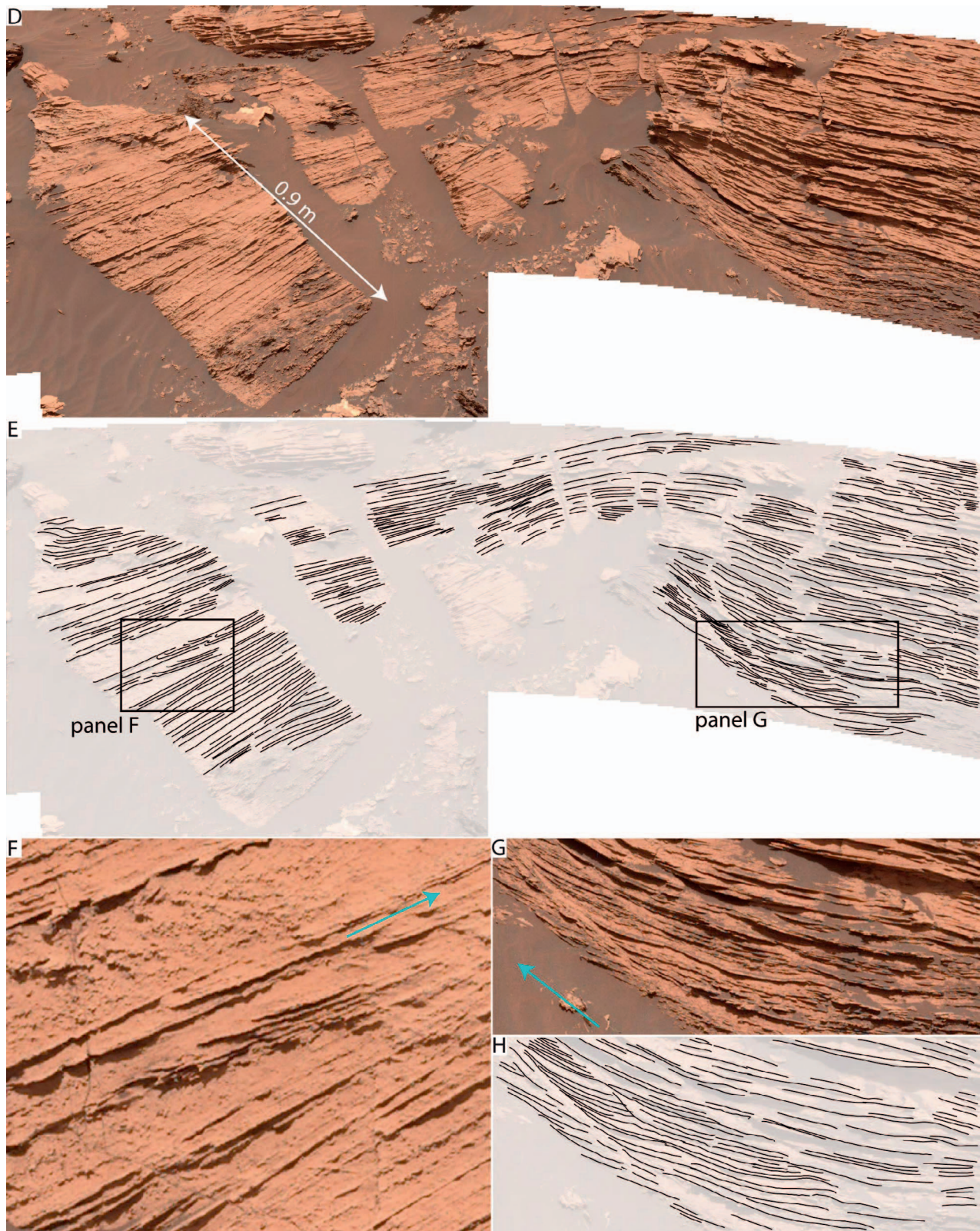


FIG. 5.—Continued.

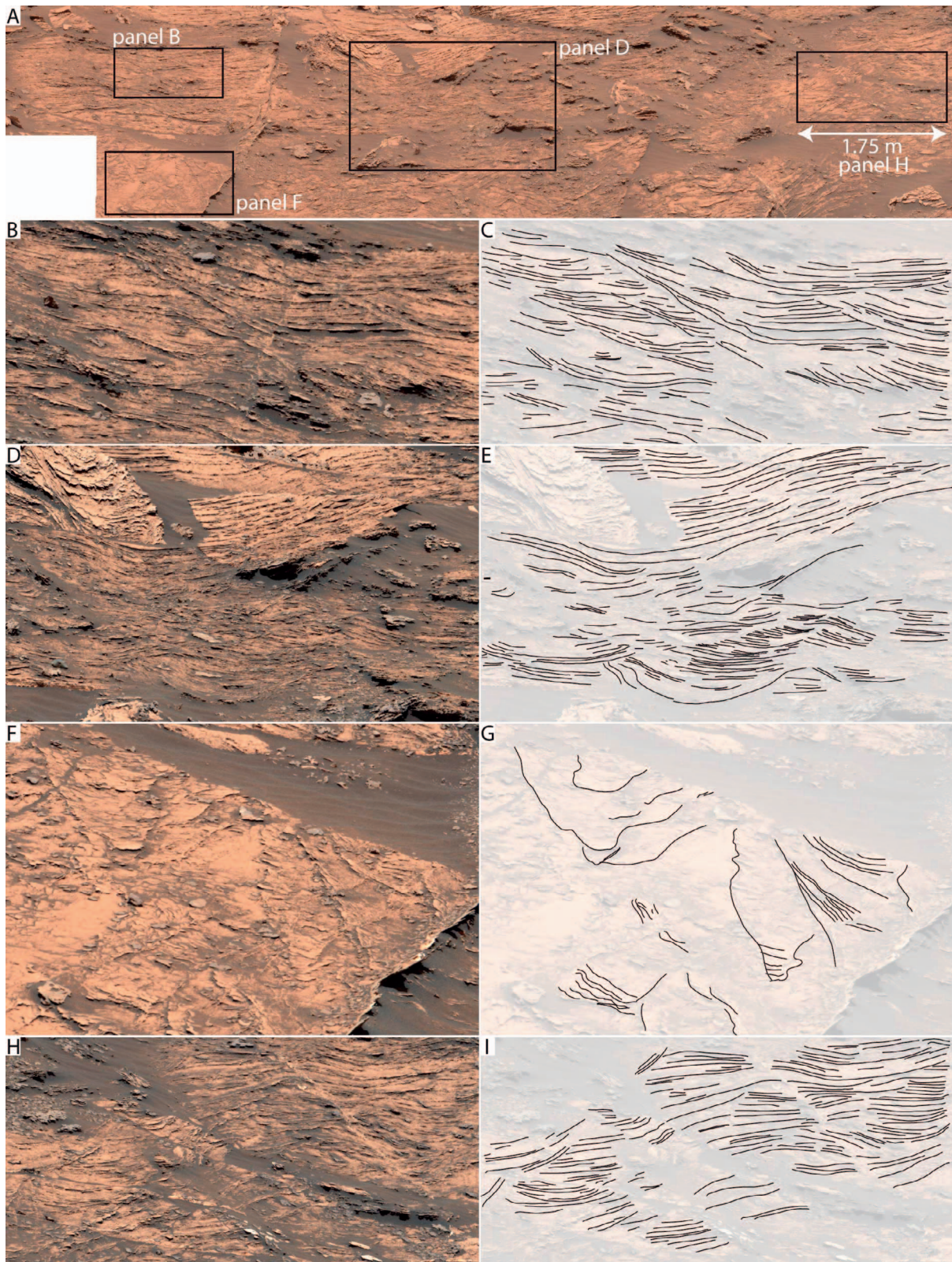


FIG. 6.—A) Planview trough cross beds along a surface dipping  $10\text{--}20^\circ$  at the western flank of Mont Mercou (mcam16100, mission sol 3083, looking southeast). Boxes show the locations of Parts B–H. We measured paleotransport directions by measuring trough axes. B–I) Images and interpretations highlighting truncation surfaces and south-concave cross strata (Mastcam image credit: NASA/Caltech-JPL/MSSS).

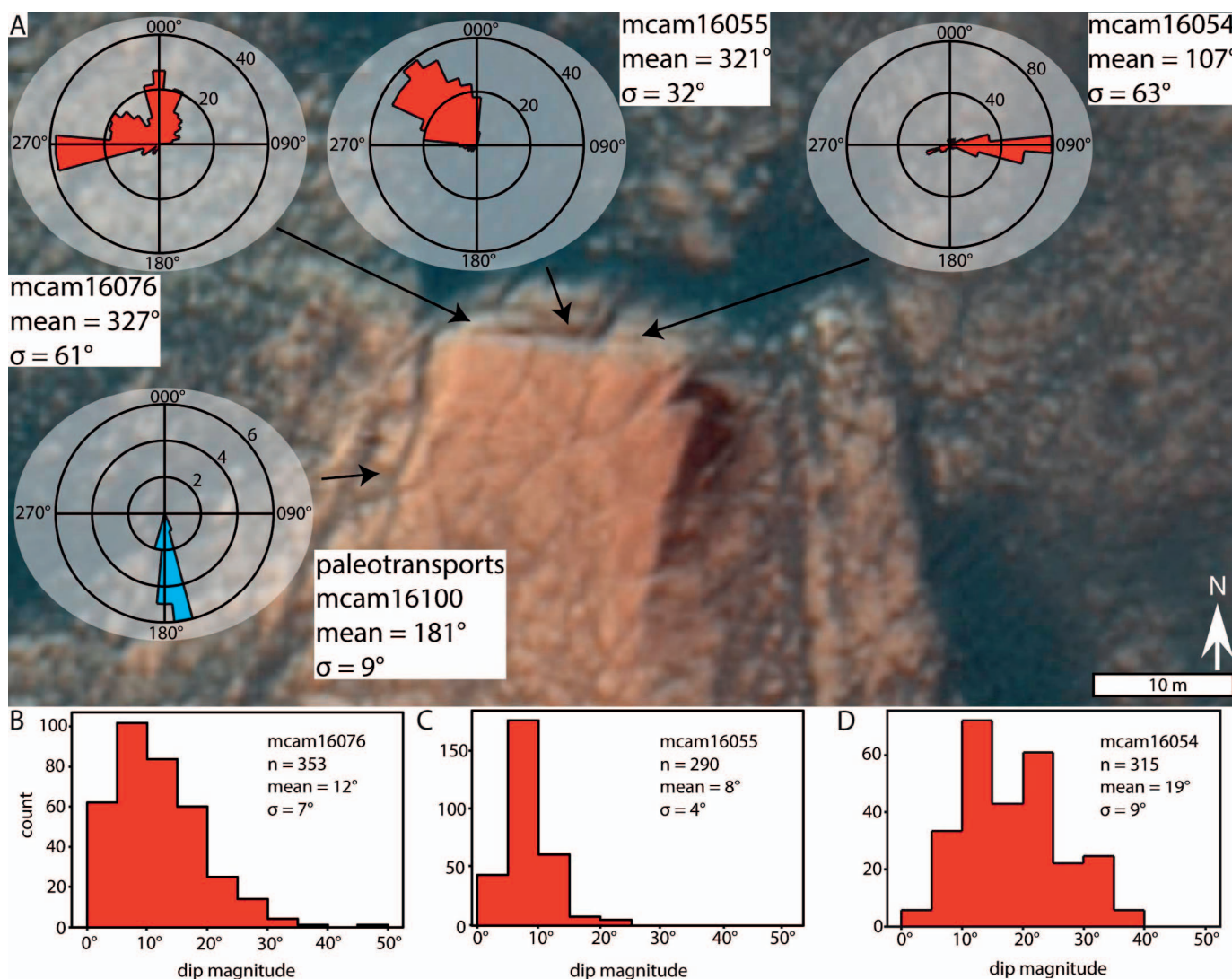


Fig. 7.—Dips and dip directions of planar beds measured from the close approaches to Mont Mercou's north-facing cliff face using Mastcam stereo data. Black arrows originate from rose diagrams and point to the locations where those measurements were made. The extent of this image is shown in Figure 2A and B. **A**) Red rose diagrams show the dip directions. Note the north-convex geometry represented across the cliff face. Paleotransport directions measured from planview exposures of trough cross strata are shown in the blue rose diagram. **B–D**) Dip magnitudes from the same fitted planes.

paleo-transport (Ashworth et al. 2000; Schomacker et al. 2010; Cardenas et al. 2020). Similarly, an overwash delta behind a beach ridge may have a lobate geometry with transport oriented downslope (Neal et al. 2003) and with evidence of an adjacent beach ridge oriented perpendicular to the lobe. The beach ridge itself would not have surfaces as steeply dipping as we observed, and would likely be too high-energy an environment to form the observed draping beds (Fig. 5A, B; Vespremeanu-Stroe et al. 2016). The back (stoss slope) of an aeolian dune, if preserved, can show the same geometry and paleotransport direction as the back of a fluvial bar (Lancaster 1988; Brothers et al. 2017). The front (lee slope) of an aeolian dune would instead show convexity, except around the limb of a barchan (Bourke 2010). In this scenario, we would also expect a change in facies associated with the changing orientation of the dune crest to the wind direction and relative importance of grainflow and ripple migration shift (Hunter 1977; Eastwood et al. 2012; Zhao et al. 2021), but this was not observed. Parabolic dunes were not considered since they are typically the result of vegetation growth on a dune modifying sediment transport (Nield

and Baas 2008; Reitz et al. 2010), and thus are unlikely to be preserved in the martian sedimentary record.

Considering the change in dip orientations across the face of Mont Mercou, dip magnitudes distributed around depositional ranges, the south-southwest paleotransport direction inferred from dune trough cross strata, and the ridge shape of the exposure, we interpret the strata exposed at Mont Mercou to represent a downstream-migrating fluvial barform that had superimposed dunes migrating up the back of the bar in a river that locally flowed south. Though the geometry and paleotransport directions are also consistent with the back of an aeolian dune, preserved dune stoss slopes are rare in most environments. Preserving the backs of large aeolian dunes has been attributed to relatively extreme and unusual events, including the rapid flooding of dune fields (Kocurek et al. 2019) and burial by lava flows (Jerram et al. 2000; Waichel et al. 2008; Gaylord et al. 2021). While these situations have likely occurred on Mars (Day and Catling 2018), we did not observe independent evidence for these events. In contrast, the preservation of fluvial bar stoss slopes is common because channel abandonment during channel switching leaves riverbed topography “frozen-in-place” where it is

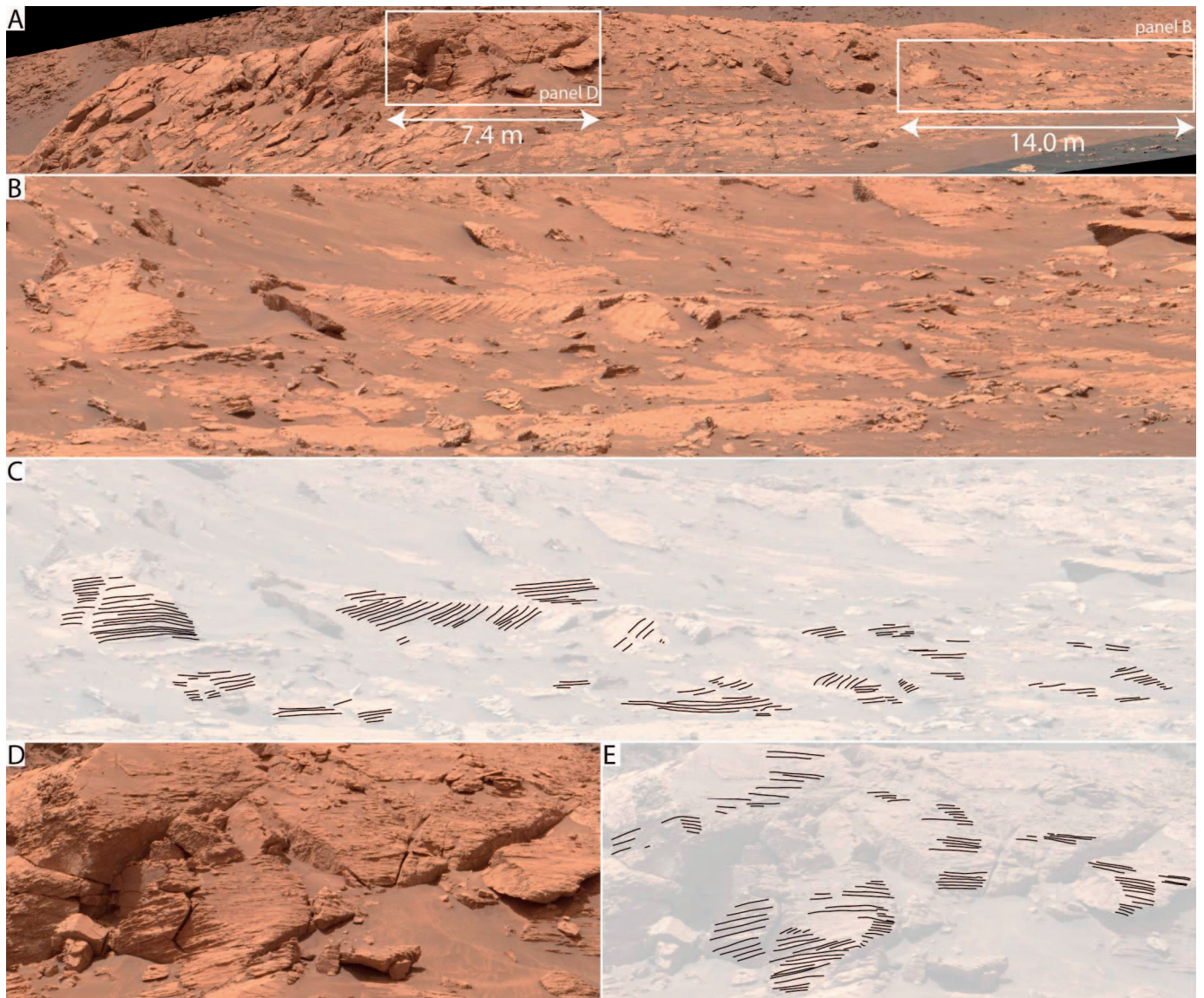


FIG. 8.—**A**) West-facing wall of the ridge east of Mont Mercou (mcam16062, mission sol 3076, looking east; location shown in Fig. 2). Boxes show the locations of Parts B and D. **B–E**) Bedding and possible cross bedding similar in scale to beds observed at Mont Mercou. Parts C and E show interpretations (Mastcam image credit: NASA/Caltech-JPL/MSSS).

later draped by overbank deposits from an adjacent channel (Mohrig et al. 2000; Jerolmack and Mohrig 2007; Toonen et al. 2012; Chamberlin and Hajek 2019; Cardenas et al. 2020). Additionally, the offset strata with decreasing offset upwards are interpreted as minor growth strata of a small syndepositional fault associated with a centimeter of offset from slumping that was likely subaqueous (e.g., Wignall et al. 2019) (Fig. 4). Though the orientation of beds and paleoflows are also consistent with a deltaic mouth bar, the narrow aspect ratio of the cross-bedded unit (20:1) is more consistent with an in-channel bar (Schomacker et al. 2010), though erosion has likely increased this ratio as there is no preserved rollover marking the top of the interpreted bar. The elongate erosional morphology of Mont Mercou and the adjacent ridge also suggests that these strata were part of channel belts (Fig. 2). Channel belts are elongate sedimentary deposits recording the migration and aggradation of river channels (Friend et al. 1979; Bridge and Tye 2000; Jerolmack and Mohrig 2007). Across Mars, partially eroded channel belts form fluvial ridges with similar topographic expressions (Burr et al. 2009; Williams et al. 2013b; Davis et al. 2019;

Balme et al. 2020; Dickson et al. 2020). From orbit, fluvial ridges are readily identified by their continuity, being persistently mappable for tens and even hundreds of kilometers. The ridges in the Mercou member, in contrast, are truncated at their north ends, and are presumably incompletely exhumed at their south ends where topography continues to rise towards the top of Aeolis Mons (Fig. 2).

The bar height was likely at least as tall as the thickness of the cross-bedded interval, 0.64 m. We emphasize that this is a minimum estimate due to possible reworking during channel filling, since any topographic rollover representing the top of the bar is absent (Mohrig et al. 2000; Alexander et al. 2020). As a further limit, the outcrop itself may not completely expose the cross-bedded unit, as we did not observe its bottom contact. Even if bar height were better constrained here, bar heights can equal anywhere from 1/3 to 1 times mean bankfull channel depth (Mohrig et al. 2000; Alexander et al. 2020). Thus, we estimate the paleo-channel was about 1–2 m deep.

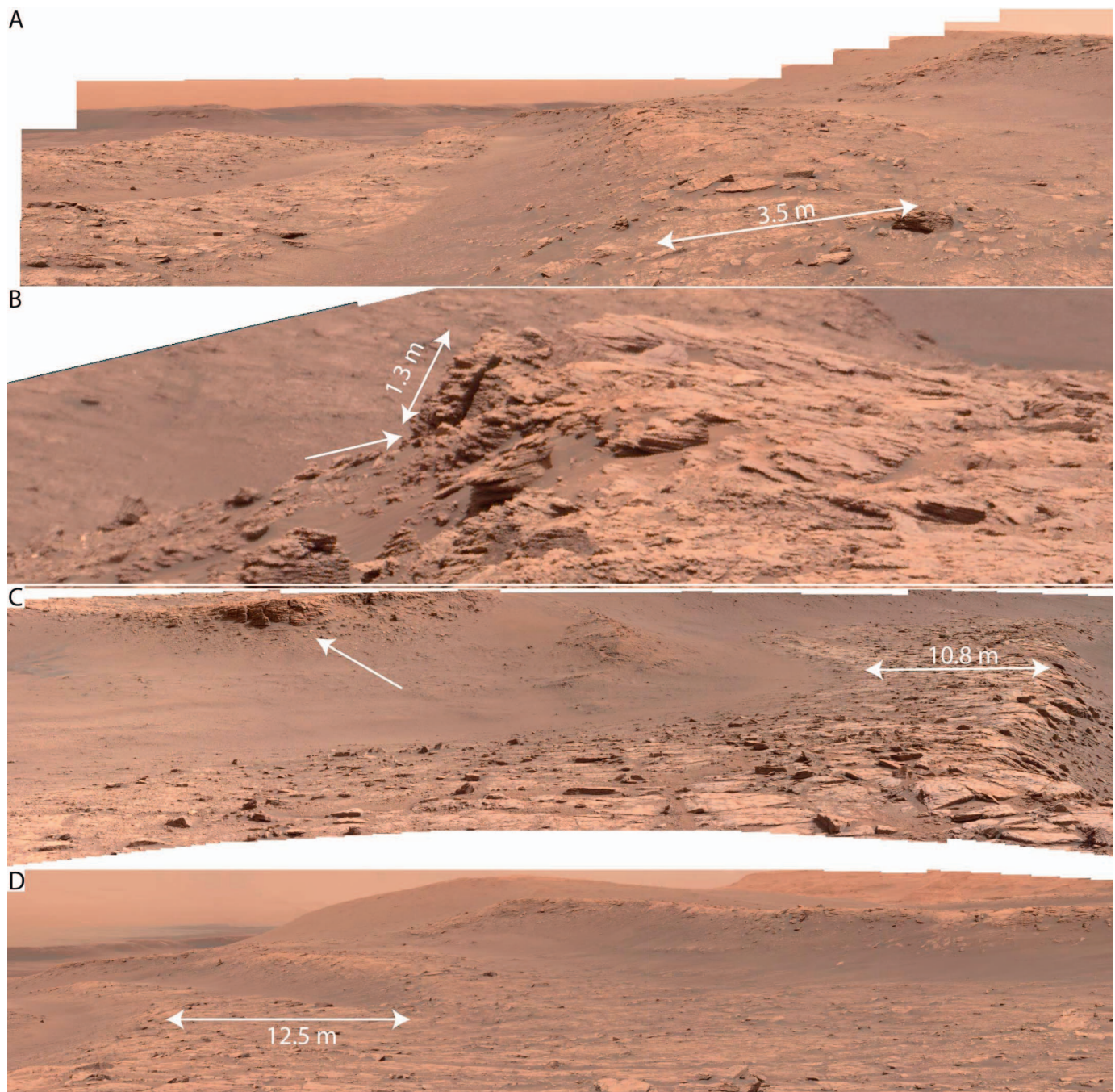


FIG. 9.—Erosional morphology of the Glasgow member exposures. **A)** A series of topographic slopes and benches define the region, with exposures limited to bench edges and tops (mcam15328, mission sol 2938, looking east). **B)** Bench edges can be diffuse as in Part A, or form steep cliffs with minor overhangs as shown here and in Part C (white arrows; mcam15351, mission sol 2943, looking north). **C)** Bench tops tend to provide relatively continuous exposures of primarily planar bedding (mcam15355, mission sol 2943, looking south). **D)** Bench tops have relief on the meter scale (Mastcam image credit: NASA/Caltech-JPL/MSSS) (mcam15302, mission sol 2933, looking east).

#### *Glasgow Member Interpretation*

We interpret the eastern Glasgow member exposures at the benches to be either stacks of point-bar deposits or deltaic mouth bars. Most of the exposures are defined by broadly dipping planar beds and laminae, but locally we infer changes in dip to be associated with low-angle trough cross stratification (Fig. 10). Low-angle trough cross strata are common in some fluvial deposits (Fielding 2006) and can take on a more planar look

depending on viewing orientation (Fig. 14), similar to what we observed in the Glasgow member (Fig. 10). The low-angle cross strata may be associated with the preferential preservation of dune toesets (Fig. 14). Subaqueous dunes with shallowly dipping lee slopes are found in relatively deep rivers on Earth (Kostaschuk and Venditti 2019; Cisneros et al. 2020) and would likely produce low-angle cross strata, but it is unknown if such dunes would form in shallow (< 2.5 m; Cisneros et al. 2020) martian channels.

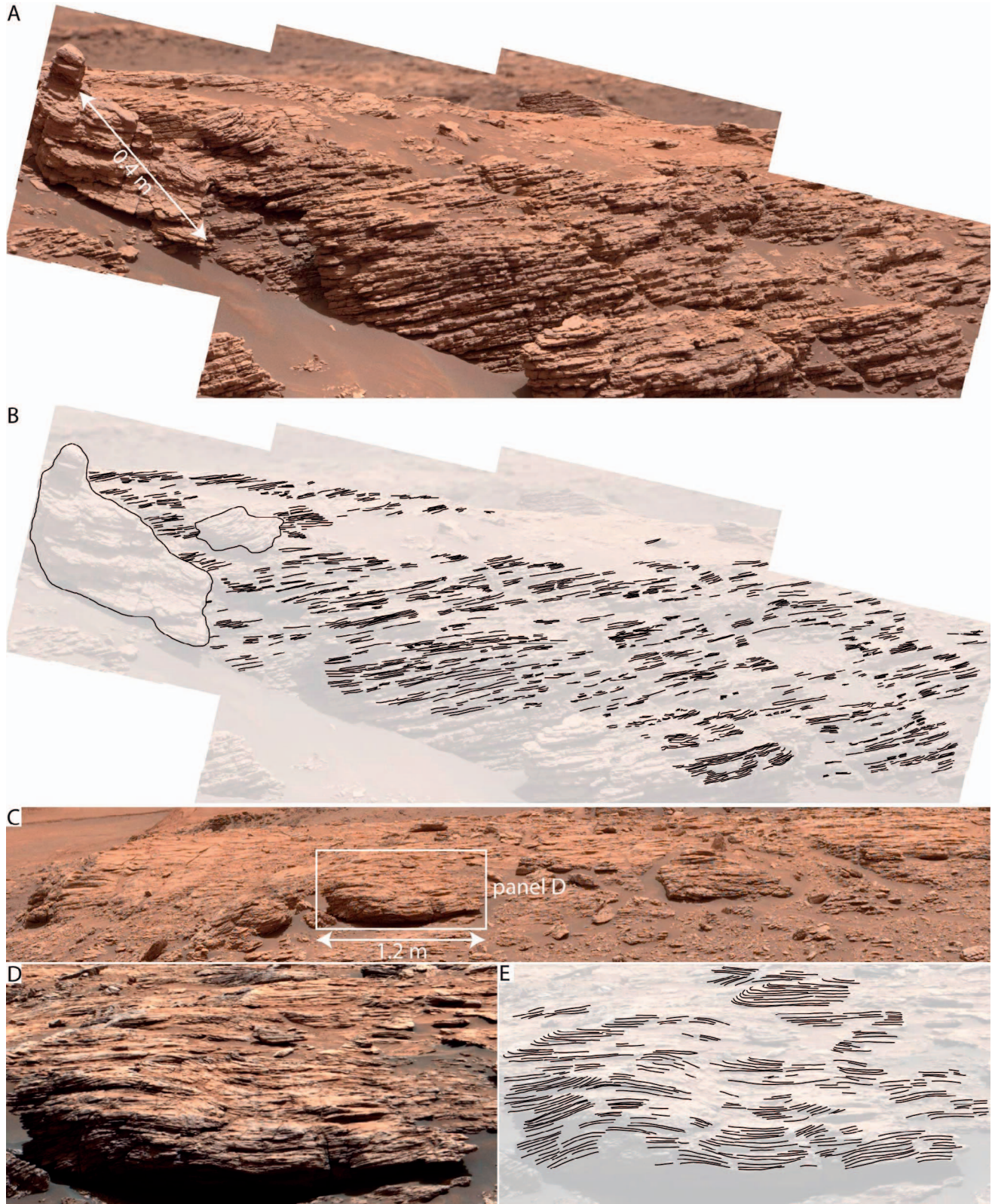


FIG. 10.—Sedimentology of the Glasgow member. **A)** Planar beds in a bench-forming exposure (mcam15353, mission sol 2943, looking southeast). **B)** Interpretation shows strata are consistently oriented. **C)** Bench-forming exposure with planar beds as well as curved strata (mcam15298, mission sol 2933, looking southeast). A box shows the location of Part D. **D)** Curved strata. **E)** Interpretation highlights a few truncation surfaces and the local variability in dip direction commonly associated with trough cross strata. **F)** Low-angle cross beds (mcam15342, mission sol 2940, looking east). Boxes show the location of other parts. **G–L)** Zoom ins to Part F, with interpretations highlighting the low-angle cross bedding (Mastcam image credit: NASA/Caltech-JPL/MSSS).

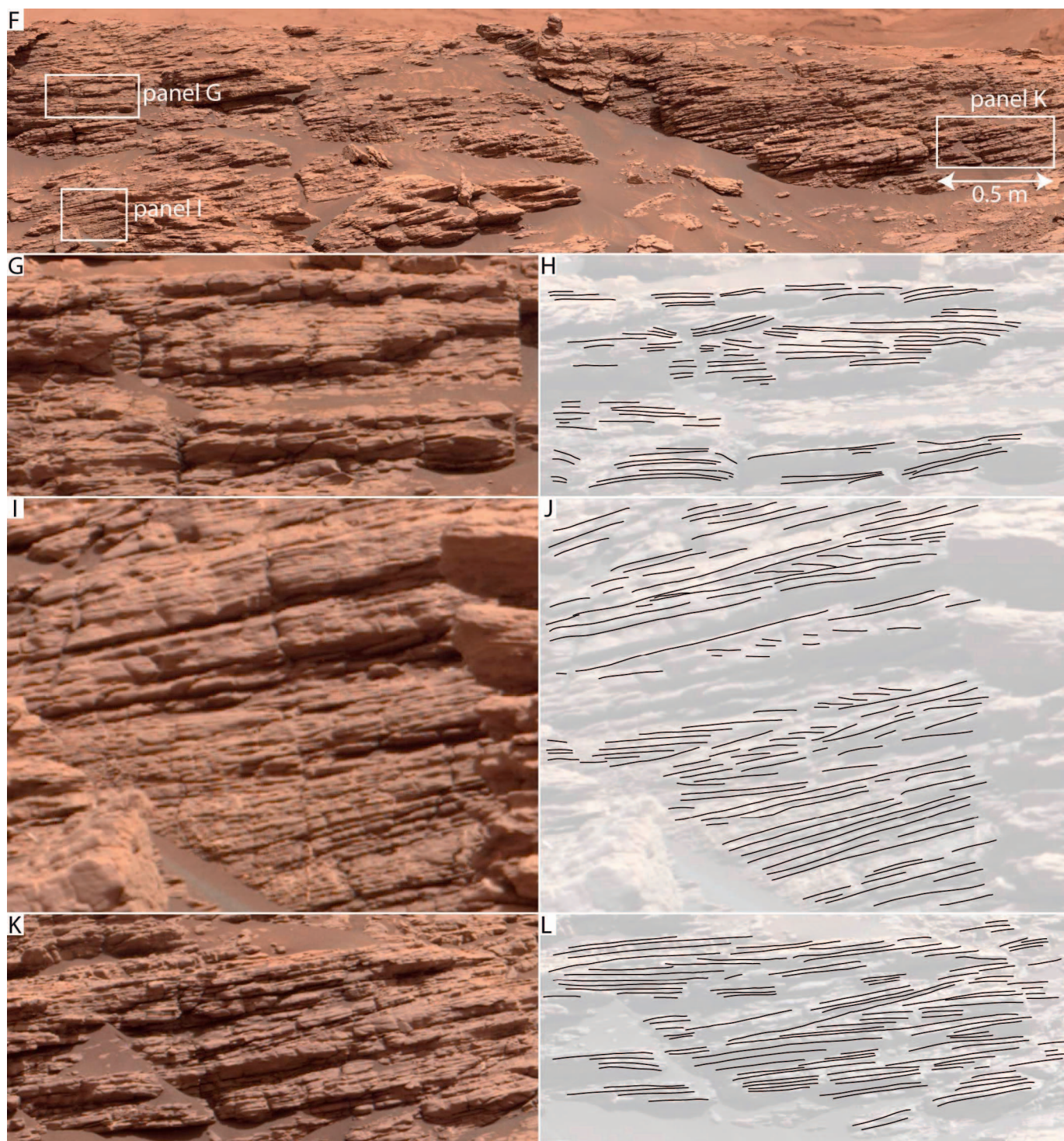


FIG. 10.—Continued.

We infer the scarp-and-slope morphology to indicate that there are weaker, unexposed rocks between the exposed bench-forming strata, though we are limited to inference as no observations of the lithology between bench-forming strata were made. This is a morphology that has been observed elsewhere in Gale crater and has been attributed to the differential aeolian erosion of stacked beds with different lithologies (Day and Kocurek 2016), including the sandstone–mudstone contacts observed

at Yellowknife Bay (Farley et al. 2014) and Pahrump Hills (Grotzinger et al. 2015), and in alluvial sequences on Earth (Hayden et al. 2019; Chamberlin and Hajek 2022). Stacked and shingled channel belts with overbank strata in between are common components of alluvial sequences because unoccupied channels frequently attract later flow (Mohrig et al. 2000; Aslan et al. 2005; Jerolmack and Paola 2007; Hajek et al. 2010; Chamberlin and Hajek 2015; Reitz et al. 2015; Owen et al. 2015; Cardenas

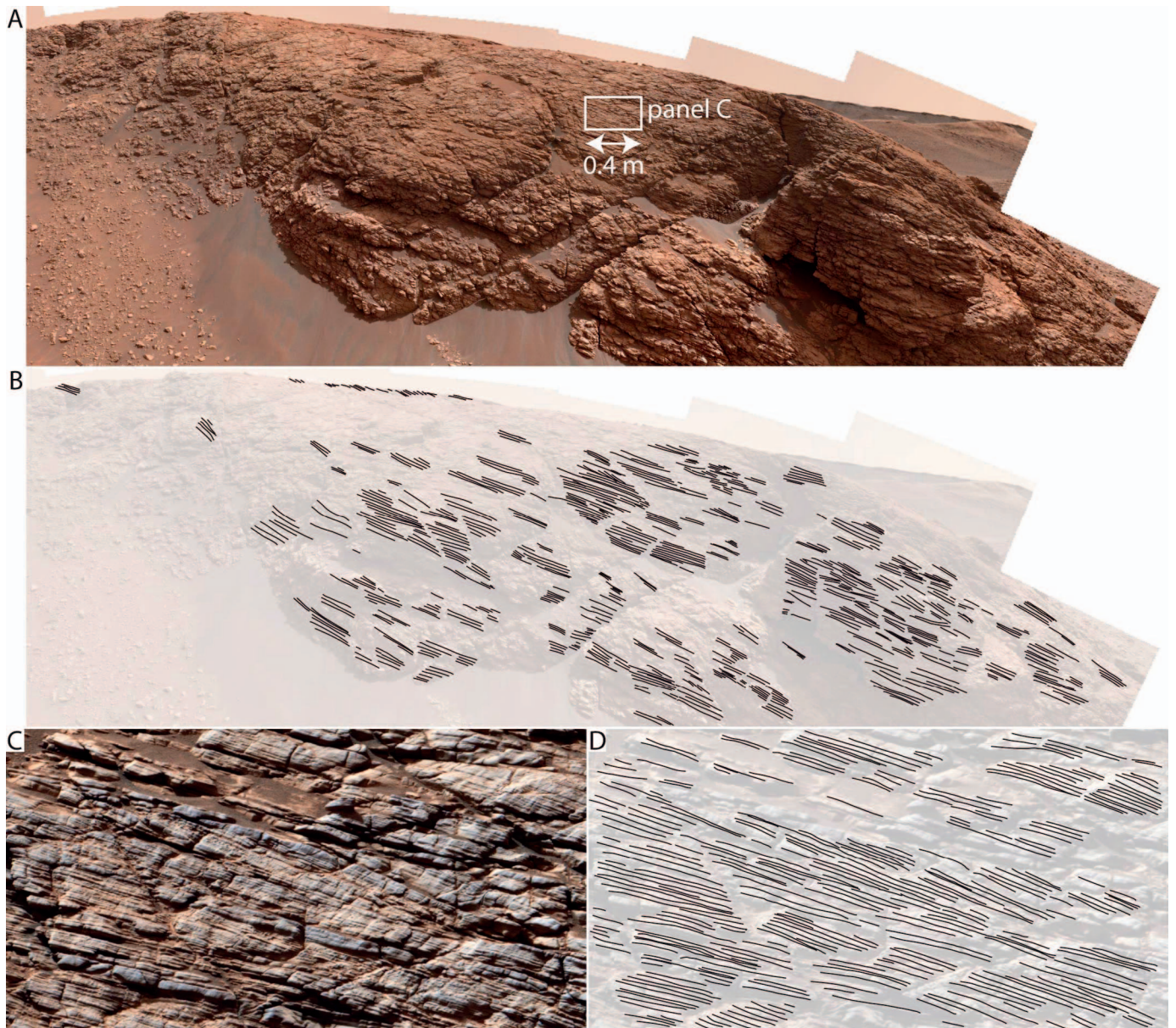


Fig. 11.—**A**) Planar bedding at the Maybole outcrop, and the location of Part C (mcam15253, mission sol 2923, looking south). **B**) Interpretation shows the consistency of orientations. **C**) Zoom in to Maybole. **D**) Interpretation of Part C shows bedding in the central part of the panel is at a low angle to surrounding beds (Mastcam image credit: NASA/Caltech-JPL/MSSS).

et al. 2020; Sahoo et al. 2020), though stacking could potentially occur randomly and not reflect reoccupation (Chamberlin and Hajek 2015). Low accommodation and low supply of fine sediment could drive channel-belt clustering without reoccupations (Chamberlin and Hajek 2015 2022), but given the excess of accommodation in the crater (the Carolyn Shoemaker formation is several kilometers below the modern-day crater rim; Fig. 1) and the geomorphic indicators of mudstones between bench-forming sandstones, we do not factor these into our interpretations. Across Mars, and on Earth as well, erosion of alluvial strata with well-cemented sandstones and more diffuse mudstones can result in sinuous ridges with steep cliff faces that transition to shallow hillslopes formed from overbank deposits (Williams et al. 2007, 2013b; Burr et al. 2009, 2010; Hayden et al. 2019; Hayden and Lamb 2020; Dickson et al. 2020; Cardenas et al. 2022). The presence of variable lithologies would be consistent with the presence

of overhanging capping units at some places, although gentler transitions from benchtop to hillslope define these boundaries as well (Fig. 9).

At the Glasgow member outcrops, the trends in dip orientation and the curved geometry of bench-forming strata are consistent with stacked fluvial point bars, downstream-migrating bars, and delta mouth bars (Fig. 12). Point bars are located at the inner bends of meandering channels and, unlike downstream migrating bars, they accrete into the channel orthogonal to the main flow direction and thus show net transport directions at oblique angles to bar dip directions (Dietrich and Smith 1983; Ikeda and Parker 1989; Mason and Mohrig 2018, 2019a). Point bars are associated with a suite of sedimentary structures, including planar beds, ripple laminae, climbing ripples, and dune cross beds (Edwards et al. 1983; Mason and Mohrig 2019b; Hagstrom et al. 2019). Importantly, the migration of the same channel bend can occur over repeated river reoccupations, such that

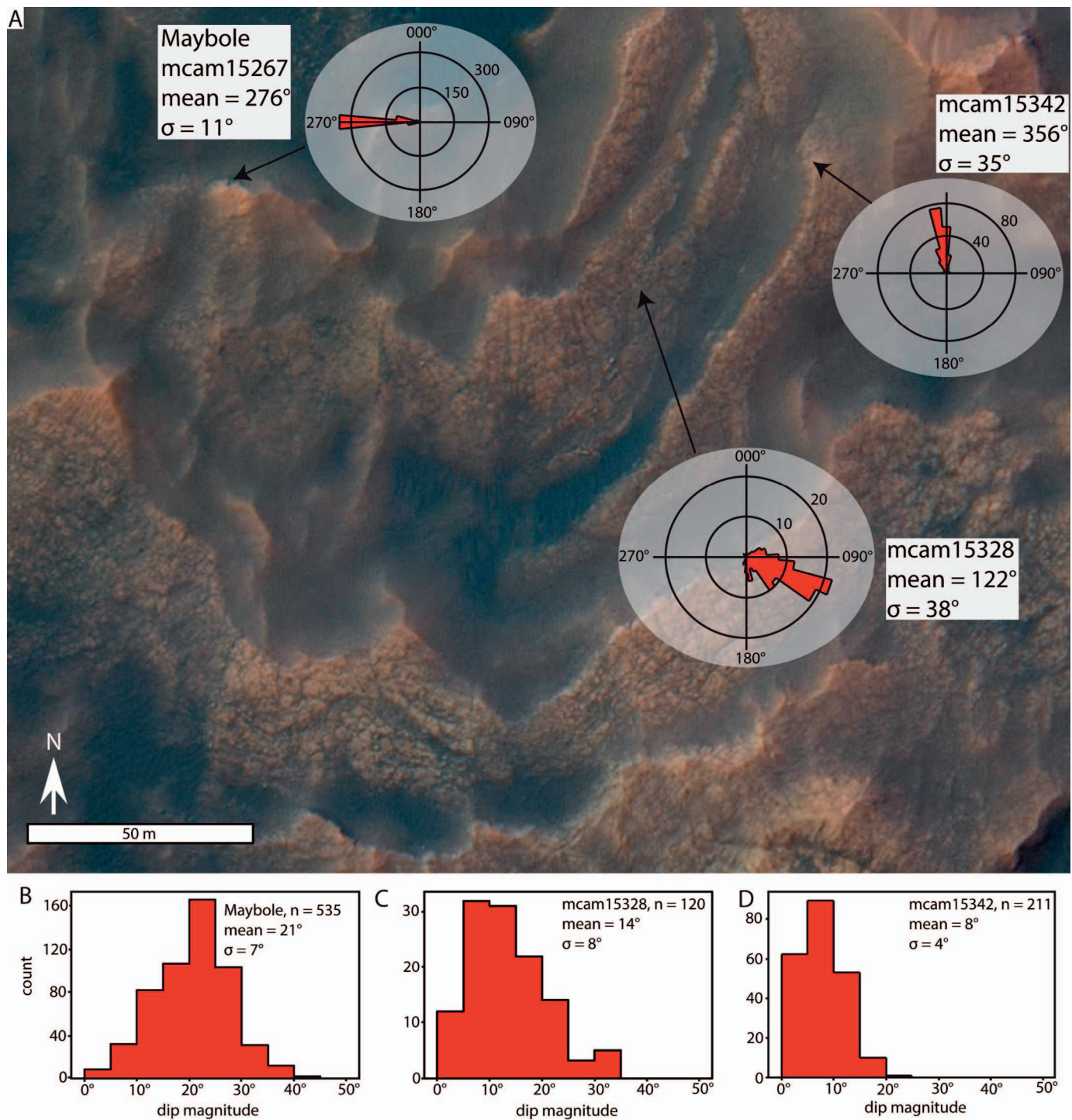


FIG. 12.—Dips and dip directions of planar beds measured from three locations across the Glasgow member exposures. Black arrows originate from rose diagrams and point to the location where those measurements were made. The extent of this image is shown in Figure 2A and D. **A**) Red rose diagrams show the dip directions. Based on the three locations measured, dip directions change across the exposure, dipping away from bench edges for the two western exposures, and down the nose of a dipping bench top at the eastern location, altogether forming a roughly south-convex shape. Paleotransport directions measured from planview exposures of trough cross strata are shown in the blue rose diagram. **B–D**) Dip magnitudes from the same fitted planes.

multiple stacked channel belts may deposit similarly shaped point bars at the same location with the same accretion direction (Cardenas et al. 2020). Unlike in the Mercou member, we lacked a clear indicator of paleoflow direction in the Glasgow member to compare to bar dip directions and

directly test whether they are point bars versus downstream-migrating bars or mouth bars (Miall 1977; Edwards et al. 1983; Wu et al. 2015, 2016; Almeida et al. 2016; Cardenas et al. 2020). Although we could not constrain the paleo-flow direction relative to the dip of the bar surfaces, the

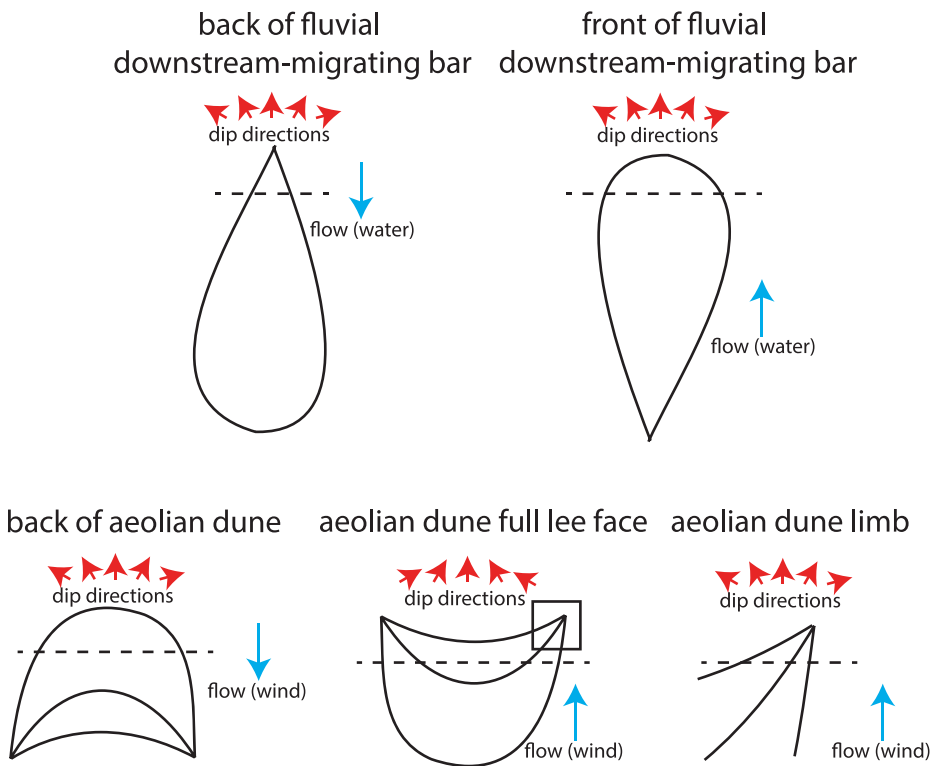


FIG. 13.—Hypotheses to test for the large-scale sedimentary feature preserved at Mont Mercou using bedding plane orientations and paleotransport directions measured from cross bedding.

125 m width of the cusate bench structure is about an order of magnitude wider than the 21 m wide Mont Mercou (Fig. 2). This difference in width suggests that the strata exposed along bench edges preserve a larger structure than at Mont Mercou, more consistent with point bars or deltaic mouth bars rather than a downstream-migrating bar as interpreted at Mont Mercou, assuming that channel dimensions were not drastically different between the two outcrops.

Wind erosion tends to cut cusate forms into steeply exposed bedrock. This is evident across Vera Rubin ridge and along the stepped exposed bedrock in the region (Stack et al. 2022). However, the hypothesis that the benches may record channel bars raises the possibility that the cusp shape of the benches could reflect instead the traces of point bars in a meandering river system. The observed agreement between the curved planview bench geometry and dip directions (Fig. 12) suggests that the curved geometry of the benches might reflect the curved geometry of point bars, though we acknowledge that there was not enough Mastcam stereo coverage to test this hypothesis along full benchtop traverses. Point bars have planform deposit geometries that can reflect, in some cases, the curvature of the paleo-channel (Wu et al. 2015; Jacobsen and Burr 2018; Hayden and Lamb 2020). This occurs because point bars accrete into channels as channels migrate, creating stratigraphic packages that broadly track channel migration. But problems can arise because the planform geometry of outcrops is erosional and may not be related to underlying lithology, or because differential erosion has modified the shape (Hayden et al. 2019, 2021; Hayden and Lamb 2020). These concerns are mitigated by the match between bench curvature and stratigraphic dip directions, but other types of bars can give similar relationships; thus, this is not a diagnostic test of meandering. Nonetheless, the planform shape of delta mouth bars is not thought to be related to channel curvature, since mouth bars do not grow at channel bends (Edmonds and Slingerland 2007; Daniller-Varghese et al. 2020).

As a self-consistency test for the point bar hypothesis, we calculated paleo-channel depth using the radius of curvature of a bench top to see if it matched the paleo-channel depth at Mont Mercou. If the benches expose

point bars and if the paleo-channel depth does not vary between the Glasgow and Mercou members, the reconstructed depths should be similar between the members. We fit a circle to the top of the most continuous bench in a GIS. We calculated the radius of that circle at 60 m and took this to be the radius of curvature of a channel bend, assuming that this curvature represented the curvature of an exhumed point bar. We used a common relationship between radius of curvature and channel-form width to calculate the width of the paleochannel,  $W$  (Williams 1986; Kite et al. 2019; Hayden et al. 2021):  $R = 1.5W^{1.12}$ . Solving for  $W$  gave a paleochannel width of 27 m. A published dataset of alluvial-river geometries on Earth shows that the median width-to-depth ratio of an alluvial channel to be 18 (Trampush et al. 2014), and it is not thought that width-to-depth ratios for martian channels should be significantly different from Earth channels (Irwin et al. 2005). Using this width-to-depth ratio gave a paleochannel depth of 1.5 m, similar to our independent estimate of channel depth from the Mercou member and supporting the point-bar interpretation. If we instead used a different width-to-depth ratio of 12.5 observed in nonvegetated rivers on Earth (Ielpi and Lapôtre 2020), we would calculate channel depths at the Glasgow member outcrops to be slightly deeper at 2.2 m. Channels are expected to be deeper around bends where point bars develop (Dietrich and Smith 1983; Bridge and Mackey 1993). Thus, it remains plausible that the Glasgow member outcrops could represent point bars in channels that had a geometry similar to the Mercou member. In this scenario, the 2–4 m vertical spacing between bench tops could represent the thickness of a package of fine-grained overbank strata and a channel belt, with the entire exposure here representing four distinct stacked belts. However, none of these observations contradict the stacked-mouth-bars interpretation. The results from the radius-of-curvature comparison would have to be coincidental, but a mouth bar would be consistent with the wave-ripple structures identified about half a kilometer to the west and in a loose rock near the top of the benches (Fedo et al., in review; Rubin et al. 2022). In this scenario, the observed lithologic variability would represent interbedded lacustrine mudstones between

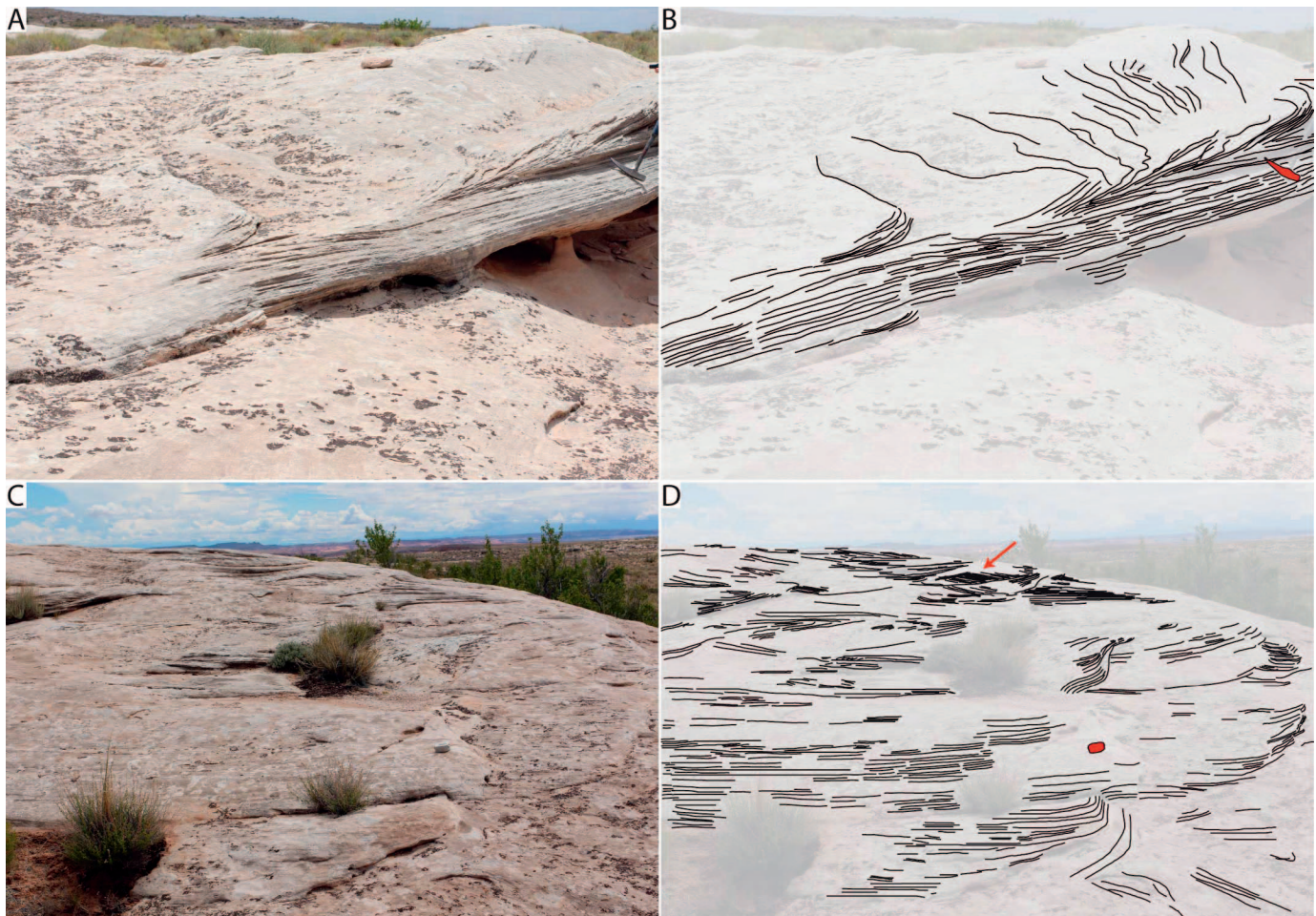


FIG. 14.—Low-angle crossbedding in an ancient point bar of the Jurassic Morrison Formation, south of Green River, Utah, USA. **A)** Vertical and planview exposure of high-angle cross beds preserved at the preserved top of a bar surface, with a downstream transition into preserving only low-angle toe sets. Hammer head for scale. **B)** The interpretation highlights the similarity in plane bed and low-angle cross strata. Hammer head for scale is in red. **C)** Three-dimensional exposure of bar strata. **D)** Interpretation shows this exposure is composed of steep and low-angle cross strata and low-angle truncation surfaces. Brunton compass in red for scale. Red arrow points to steep cross strata.

stacked mouth bars rather than floodplain deposits (Schomacker et al. 2010).

We tested several alternative hypotheses to bars, but none explained both 1) the observed dip variability and 2) the bench topography. One alternative hypothesis is that the south-convex dip direction pattern represents a structure akin to a plunging anticline or a series of relay ramps. Significant non-plate-tectonic deformation can occur in thick sedimentary accumulations (Treviño and Vendeville 2008; Armstrong et al. 2014). However, while fractures in the benches exist throughout, they rarely show offset and, where they do, it is on the order of centimeters, and not enough to explain the observed variability in dip magnitudes. Additionally, the wide distribution of dip magnitudes (Figs. 7, 12) is not consistent with the regional tilting of beds that were originally horizontal. A second alternative hypothesis is that the strata are undeformed, and that the bench-and-slope morphology was set by spatially variable diagenesis in a lithologically homogeneous sequence. However, the diagenetic mechanism alone cannot explain the observed dip magnitudes or dip directions. A third alternative hypothesis is that the benches represent early-stage wind-eroded bedforms, which are common in adjacent parts of the crater (Stack et al. 2022), and are unrelated to the barform stratigraphy. The bar interpretation better explains the match between the cusp shape and bedding orientations (Fig. 12) and the inferred variability in lithology between bench margin and

hillslope (Fig. 9). A fourth alternative hypothesis is that the pattern of dips represents a delta front with a lobate clinoform. Such structures have been observed about 400 m lower in Gale's stratigraphy (Grotzinger et al. 2015) and in remote sensing data across the planet (DiBiase et al. 2013; Goudge et al. 2017; Hughes et al. 2019; Tebolt and Goudge 2022). However, delta-front clinoforms on Mars typically exhibit their lobate geometry over several kilometers (Hughes et al. 2019) rather than the 100 m observed here and in point bars elsewhere on the planet (Goudge et al. 2018; Jacobsen and Burr 2018; Hayden and Lamb 2020; Mangold et al. 2021).

#### *Shallowing Upward: Climatically Forced or Natural Variability?*

The alluvial and possibly coastal strata in the Carolyn Shoemaker formation form a shallowing-up sequence recording the progradation of a coastal zone over subaqueous Murray accumulations (Caravaca et al. 2022). Two scenarios may explain this sequence, and while we do not make an interpretation here, both could be tested through observation of the strata Curiosity will observe on its continued ascent route up Aeolis Mons.

In one scenario, shoreline progradation from the crater rim towards the center of the crater was coupled with the shrinking lateral extent and filling-in of the Gale lake system. A drying climate where water flux into the crater is exceeded by water loss in the crater, due to either evaporation or ground-

water loss, could explain a shrinking lake, and would be consistent with the drying interpreted by the sulfate-rich strata above this position (Milliken et al. 2010; Horvath and Andrews-Hanna 2021). Essentially, this scenario has Gale's ancient coastal fluvial systems transitioning to a megafan setting lacking a downstream body of standing water (Horton and DeCelles 2001; Weissmann et al. 2010; Hartley et al. 2010). This is a sequence stratigraphic interpretation of the stratigraphy, where all shallowing and deepening was driven by external forcings (Wagoner et al. 1988). However, the progradation of the fluvial system recorded here may also simply represent natural variability in the geometry of the shoreline without any change in lake level or any other external forcing (Galloway 1989; Kim et al. 2006). For instance, this sequence could record the progradation of the fluvial system into the lake under steady or even rising lake level (Porębski and Steel 2006; Chadwick and Lamb 2021). In this case, strata exposed higher on Aeolis Mons may either be fluvial and not record any significant drying upsection, or strata may transition back to sublacustrine should channel switching occur and route sediment elsewhere in the crater. Indeed, other craters with 3D exposures of deltas and fans show evidence that rivers avulsed several times during crater filling (Wood 2006; Pondrelli et al. 2008; Irwin et al. 2015; Goudge et al. 2018). Moreover, it should be expected that any shoreline in Gale crater had significant three dimensionality that evolved over time. Shorelines and lakes are low-sloping sedimentary environments, such that any local variability in sediment deposition can create relief and three-dimensionality (Straub et al. 2009). These hypotheses can be tested moving forward.

The question these hypotheses explore is whether the Carolyn Shoemaker rivers consistently flowed into standing water. This question has potentially planet-scale implications, as the Carolyn Shoemaker formation occurs at a transitional zone observed at Gale and across the planet from clay-bearing stratigraphy to sulfate-bearing stratigraphy (Milliken et al. 2010). This transition is thought to record the gradual drying of the martian climate (Bibring et al. 2006; Ehlmann et al. 2011; Horvath and Andrews-Hanna 2021), a hypothesis which could directly be tested at Gale crater to see whether the sedimentary deposits also record drying. A shallowing-up sequence at one location does not necessarily imply regional drying (Galloway 1989; Kim et al. 2006), so additional observations up-section are required.

#### CONCLUSION

We present measurements of bedding orientations made from Mastcam stereo images and sedimentary structures of Glasgow and Mercou members of the Carolyn Shoemaker formation overlying the lacustrine Murray formation. At both locations, the suites of sedimentary structures, larger-scale structure, and erosional morphology are most consistent with a series of exhumed bars formed in ancient rivers and possibly coastal zones. The record of fluvial progradation over the Murray formation lacustrine mudstones could represent a climatic shift associated with the drying and shrinking of the Gale lake system and the transition of coastal rivers to megafan rivers, or it could represent the inherent variability over time in sediment-routing rivers independent of climate change. With the strata analyzed here as a baseline for new comparisons, these hypotheses could be tested as the Curiosity rover continues to ascend the flanks of Aeolis Mons by looking for evidence for drying in stratigraphically higher rocks. Given the coupling of this change in depositional setting with a planet-scale geochemical signal thought to record the drying of the planet, there is an opportunity to test this important martian geochemical hypothesis against sedimentological evidence.

#### ACKNOWLEDGMENTS

We would like to thank Journal of Sedimentary Research Editor Kathleen Marsaglia, Associate Editor John Gillies, and Technical Editor John Southard

for the handling of our manuscript. Reviewers Ellen Chamberlin and Chenliang Wu are thanked for their thoughtful comments that helped improve the text and figures. We acknowledge Ashwin Vasavada and MSL science-team members and collaborators who participated in operations during these imaging campaigns, and members of the MSL Sedimentology and Stratigraphy Working Group for discussions. We thank the Malin Space Science Systems team for their efforts. BTC thanks Jay Dickson for assistance in Caltech's Murray Lab for Planetary Visualization, where the analysis was performed, as well as Tim Goudge, Hima Hassenruck-Gudipati, Cory Hughes, Joe Levy, Woong Mo Koo, David Mohrig, and Feifei Zhao for their work at the Morrison Formation between 2015 and 2018. GC was supported in France by French Agence Nationale de la Recherche (ANR) under the contract ANR-16-CE31-0012 entitled Mars-Prime, and by the French space agency CNES under convention CNES 180027.

Data used in this manuscript are available at the Caltech Data Repository, <http://dx.doi.org/10.22002/D1.20044>.

#### REFERENCES

- ALEXANDER, D.A., DEEN, R.G., ANDRES, P.M., ZAMANI, P., MORTENSEN, H.B., CHEN, A.C., CAYANAN, M.K., HALL, J.R., KLOCHKO, V.S., PARISER, O., STANLEY, C.L., THOMPSON, C.K., AND YAGI, G.M., 2006, Processing of Mars Exploration Rover imagery for science and operations planning: *Journal of Geophysical Research, Planets*, v. 111, doi:10.1029/2005JE002462.
- ALEXANDER, J.S., McELROY, B.J., HUZURBAZAR, S., AND MURR, M.L., 2020, Elevation gaps in fluvial sandbar deposition and their implications for paleodepth estimation: *Geology*, v. 48, p. 718–722, doi:10.1130/G47521.1.
- ALMEIDA, R.P., FREITAS, B.T., TURRA, B.B., FIGUEIREDO, F.T., MARCONATO, A., AND JANIKIAN, L., 2016, Reconstructing fluvial bar surfaces from compound cross-strata and the interpretation of bar accretion direction in large river deposits: *Sedimentology*, v. 63, p. 609–628, doi:10.1111/sed.12230.
- ARMSTRONG, C., MOHRIG, D., HESS, T., GEORGE, T., AND STRAUB, K.M., 2014, Influence of growth faults on coastal fluvial systems: examples from the late Miocene to Recent Mississippi River Delta: *Sedimentary Geology*, v. 301, p. 120–132, doi:10.1016/j.sedg.2013.06.010.
- ASHWORTH, P.J., BEST, J.L., RODEN, J.E., BRISTOW, C.S., AND KLAASSEN, G.J., 2000, Morphological evolution and dynamics of a large, sand braid-bar, Jamuna River, Bangladesh: evolution of a large sand braid-bar: *Sedimentology*, v. 47, p. 533–555, doi:10.1046/j.1365-3091.2000.00305.x.
- ASLAN, A., AUTIN, W.J., AND BLUM, M.D., 2005, Causes of river avulsion: insights from the late Holocene avulsion history of the Mississippi River, U.S.A.: *Journal of Sedimentary Research*, v. 75, p. 650–664, doi:10.2110/jst.2005.053.
- BALME, M.R., GUPTA, S., DAVIS, J.M., FAWDON, P., GRINDROD, P.M., BRIDGES, J.C., SEFTON-NASH, E., AND WILLIAMS, R.M.E., 2020, Aram Dorsum: an extensive mid-Noachian age fluvial depositional system in Arabia Terra, Mars: *Journal of Geophysical Research, Planets*, v. 125, no. e2019JE006244, doi:10.1029/2019JE006244.
- BANHAM, S.G., GUPTA, S., RUBIN, D.M., WATKINS, J.A., SUMNER, D.Y., EDGETT, K.S., GROTZINGER, J.P., LEWIS, K.W., EDGAR, L.A., STACK-MORGAN, K.M., BARNES, R., BELL III, J.F., DAY, M.D., EWING, R.C., LAPÔTRE, M.G.A., STEIN, N.T., RIVERA-HERNANDEZ, F., AND VASAVADA, A.R., 2018, Ancient Martian aeolian processes and palaeomorphology reconstructed from the Stimson formation on the lower slope of Aeolis Mons, Gale crater, Mars: *Sedimentology*, v. 65, p. 993–1042, doi:10.1111/sed.12469.
- BANHAM, S.G., GUPTA, S., RUBIN, D.M., EDGETT, K.S., BARNES, R., VAN BEEK, J., WATKINS, J.A., EDGAR, L.A., FEDO, C.M., WILLIAMS, R.M., STACK, K.M., GROTZINGER, J.P., LEWIS, K., EWING, R.C., DAY, M., AND VASAVADA, A.R., 2021, A rock record of complex aeolian bedforms in a Hesperian desert landscape: The Stimson formation as exposed in the Murray Buttes, Gale crater, Mars: *Journal of Geophysical Research: Planets*, v. 126, no. e2020JE006554, doi:10.1029/2020JE006554.
- BEDFORD, C.C., SCHWENZER, S.P., BRIDGES, J.C., BANHAM, S., WIENS, R.C., GASNAULT, O., RAMPE, E.B., FRYDENVANG, J., AND GASDA, P.J., 2020, Geochemical variation in the Stimson formation of Gale crater: provenance, mineral sorting, and a comparison with modern Martian dunes: *Icarus*, v. 341, no. 113622, doi:10.1016/j.icarus.2020.113622.
- BERENS, P., 2009, CircStat: A MATLAB toolbox for circular statistics: *Journal of Statistical Software*, v. 31, doi:10.18637/jss.v031.i10.
- BIBRING, J.-P., LANGEVIN, Y., MUSTARD, J.F., POULET, F., ARVIDSON, R., GENDRIN, A., GONDET, B., MANGOLD, N., PINET, P., FORGET, F., on behalf of the Omega team, 2006, Global mineralogical and aqueous Mars history derived from OMEGA/Mars express data: *Science*, v. 312, p. 400–404, doi:10.1126/science.1122659.
- BOURKE, M.C., 2010, Barchan dune asymmetry: observations from Mars and Earth: *Icarus*, v. 205, p. 183–197, doi:10.1016/j.icarus.2009.08.023.
- BRIDGE, J.S., AND MACKAY, S.D., 1993, A theoretical study of fluvial sandstone body dimensions, in Marzo, M., and Puigdefabregas, C., eds., *The Geological Modelling of Hydrocarbon Reservoirs and Outcrop Analogues*: John Wiley & Sons, p. 213–236, doi:10.1002/9781444303957.ch14.

- BRIDGE, J.S., AND TYE, R.S., 2000, Interpreting the dimensions of ancient fluvial channel bars, channels, and channel belts from wireline-logs and cores: *American Association of Petroleum Geologists, Bulletin*, v. 84, p. 1205–1228.
- BROTHERS, S.C., KOCUREK, G., BROTHERS, T.C., AND BUYNEVICH, I.V., 2017, Stratigraphic architecture resulting from dune interactions: White Sands Dune Field, New Mexico: *Sedimentology*, v. 64, p. 686–713, doi:10.1111/sed.12320.
- BURR, D.M., ENGA, M.-T., WILLIAMS, R.M.E., ZIMBELMAN, J.R., HOWARD, A.D., AND BRENNAND, T.A., 2009, Pervasive aqueous paleoflow features in the Aeolis/Zephyria Plana region, Mars: *Icarus*, v. 200, p. 52–76, doi:10.1016/j.icarus.2008.10.014.
- BURR, D.M., WILLIAMS, R.M.E., WENDELL, K.D., CHOJNACKI, M., AND EMERY, J.P., 2010, Inverted fluvial features in the Aeolis/Zephyria Plana region, Mars: formation mechanism and initial paleodischarge estimates: *Journal of Geophysical Research, Planets*, v. 115, doi:10.1029/2009JE003496.
- CARAVACA, G., LE MOUÉLIC, S., MANGOLD, N., L'HARIDON, J., LE DEIT, L., AND MASSÉ, M., 2020, 3-D digital outcrop model reconstruction of the Kimberley outcrop (Gale crater, Mars) and its integration into Virtual Reality for simulated geological analysis: *Planetary and Space Science*, 182, no. 104808, doi:10.1016/j.pss.2019.104808.
- CARAVACA, G., MANGOLD, N., DEHOUCK, E., SCHIEBER, J., ZAUGG, L., BRYK, A.B., FEDO, C.M., LE MOUÉLIC, S., LE DEIT, L., BANHAM, S.G., GUPTA, S., COUSIN, A., RAPIN, W., GASNAULT, O., RIVERA-HERNÁNDEZ, F., WIENS, R.C., AND LANZA, N.L., 2022, From lake to river: documenting an environmental transition across the Jura/Knockfarril Hill members boundary in the Glen Torridon region of Gale crater (Mars): *Journal of Geophysical Research: Planets*, no. e2021JE007093.
- CARDENAS, B.T., LAMB, M.P., AND GROTZINGER, J.P., 2022, Martian landscapes carved from ancient sedimentary basins: *Nature Geoscience*, v. 15, p. 871–877, doi:10.1038/s41561-022-01058-2.
- CARDENAS, B.T., MOHRIG, D., AND GOUDGE, T.A., 2018, Fluvial stratigraphy of valley fills at Aeolis Dorsa, Mars: evidence for base-level fluctuations controlled by a downstream water body: *Geological Society of America Bulletin*, v. 130, p. 484–498, doi:10.1130/B31567.1.
- CARDENAS, B.T., MOHRIG, D., GOUDGE, T.A., HUGHES, C.M., LEVY, J.S., SWANSON, T., MASON, J., AND ZHAO, F., 2020, The anatomy of exhumed river-channel belts: bedform to belt-scale river kinematics of the Ruby Ranch Member, Cretaceous Cedar Mountain Formation, Utah, USA: *Sedimentology*, v. 67, p. 3655–3682, doi:https://doi.org/10.1111/sed.12765.
- CHADWICK, A.J., AND LAMB, M.P., 2021, Climate-Change Controls on River Delta Avulsion Location and Frequency: *Journal of Geophysical Research, Earth Surface*, v. 126, doi:10.1029/2020JF005950.
- CHAMBERLIN, E.P., AND HAJEK, E.A., 2015, Interpreting paleo-avulsion dynamics from multistory sand bodies: *Journal of Sedimentary Research*, v. 85, p. 82–94, doi:10.2110/jsr.2015.09.
- CHAMBERLIN, E.P., AND HAJEK, E.A., 2019, Using bar preservation to constrain reworking in channel-dominated fluvial stratigraphy: *Geology*, v. 47, p. 531–534, doi:10.1130/G46046.1.
- CHAMBERLIN, E.P., AND HAJEK, E.A., 2022, Fine-sediment supply can control fluvial deposit architecture: an example from the Blackhawk Formation–Castlegate Sandstone transition, Upper Cretaceous, Utah, USA: *The Sedimentary Record*, v. 20, doi:10.2110/001c.36334.
- CISNEROS, J., BEST, J., VAN DIJK, T., DE ALMEIDA, R.P., AMSLER, M., BOLDT, J., FREITAS, B., GALEAZZI, C., HUIZINGA, R., IANNIRUBERTO, M., MA, H., NITTRouer, J.A., OBERG, K., ORFEO, O., PARSONS, D., SZUPIANY, R., WANG, P., AND ZHANG, Y., 2020, Dunes in the world's big rivers are characterized by low-angle lee-side slopes and a complex shape: *Nature Geoscience*, v. 13, p. 156–162, doi:10.1038/s41561-019-0511-7.
- CLARKE, J., PAIN, C.F., AND RUPERT, S., 2020, Complex expressions of inverted and exhumed relief in central Utah, and some martian counterparts: *Physical Geography*, v. 43, p. 383–400, doi:10.1080/02723646.2020.1839161.
- DANILLER-VARGHESE, M.S., KIM, W., AND MOHRIG, D.C., 2020, The effect of flood intermittency on bifurcations in fluviodeltaic systems: experiment and theory: *Sedimentology*, no. sed.12732, doi:10.1111/sed.12732.
- DAVIS, J.M., BALME, M., GRINDROD, P.M., WILLIAMS, R.M.E., AND GUPTA, S., 2016, Extensive Noachian fluvial systems in Arabia Terra: implications for early Martian climate: *Geology*, v. 44, p. 847–850, doi:10.1130/G38247.1.
- DAVIS, J.M., GUPTA, S., BALME, M., GRINDROD, P.M., FAWDON, P., DICKESON, Z.I., AND WILLIAMS, R.M.E., 2019, A diverse array of fluvial depositional systems in Arabia Terra: evidence for mid-Noachian to early Hesperian rivers on Mars: *Journal of Geophysical Research, Planets*, v. 124, p. 1913–1934, doi:10.1029/2019JE005976.
- DAY, M.D., AND CATLING, D.C., 2018, Dune casts preserved by partial burial: the first identification of *ghost dune* pits on Mars: *Journal of Geophysical Research, Planets*, v. 123, p. 1431–1448, doi:10.1029/2018JE005613.
- DAY, M., AND KOCUREK, G., 2016, Observations of an aeolian landscape: from surface to orbit in Gale Crater: *Icarus*, v. 280, p. 37–71, doi:10.1016/j.icarus.2015.09.042.
- DEEN, R.G., AND LORRE, J.J., 2005, Seeing in three dimensions: correlation and triangulation of Mars Exploration Rover imagery, in 2005 IEEE International Conference on Systems, Man and Cybernetics, v. 1, p. 911–916, doi:10.1109/ICSMC.2005.1571262.
- DI BIASE, R.A., LIMAYE, A.B., SCHEINGROSS, J.S., FISCHER, W.W., AND LAMB, M.P., 2013, Deltaic deposits at Aeolis Dorsa: sedimentary evidence for a standing body of water on the northern plains of Mars: *Journal of Geophysical Research, Planets*, v. 118, p. 1285–1302, doi:10.1002/jgre.20100.
- DICKSON, J.L., LAMB, M.P., WILLIAMS, R.M.E., HAYDEN, A.T., AND FISCHER, W.W., 2020, The global distribution of depositional rivers on early Mars: *Geology*, v. 49, p. 504–509, doi:10.1130/G48457.1.
- DIETRICH, W.E., AND SMITH, J.D., 1983, Influence of the point bar on flow through curved channels: *Water Resources Research*, v. 19, p. 1173–1192, doi:10.1029/WR019i005p01173.
- EASTWOOD, E.N., KOCUREK, G., MOHRIG, D., AND SWANSON, T., 2012, Methodology for reconstructing wind direction, wind speed and duration of wind events from aeolian cross-strata: *Journal of Geophysical Research, Earth Surface*, v. 117, doi:10.1029/2012JF002368.
- EDGAR, L.A., GUPTA, S., AND RUBIN, D.M., ET AL., 2017, Shaler: in situ analysis of a fluvial sedimentary deposit on Mars: *Sedimentology*, v. 65, p. 96–122, doi:10.1111/sed.12370.
- EDGE, K.S., YINGST, R.A., AND RAVINE, M.A., ET AL., 2012, Curiosity's Mars Hand Lens Imager (MAHLI) Investigation: *Space Science Reviews*, v. 170, p. 259–317, doi:10.1007/s11214-012-9910-4.
- EDGE, K.S., BANHAM, S.G., BENNETT, K.A., EDGAR, L.A., EDWARDS, C.S., FAIREN, A.G., FEDO, C.M., FEY, D.M., GARVIN, J.B., GROTZINGER, J.P., GUPTA, S., HENDERSON, M.J., HOUSE, C.H., MANGOLD, N., MCLENNAN, S.M., NEWSOM, H.E., ROWLAND, S.K., SIEBACH, K.L., THOMPSON, L., VANBOMMEL, S.J., WIENS, R.C., WILLIAMS, R.M.E., AND YINGST, R.A., 2020, Extraformational sediment recycling on Mars: *Geosphere*, v. 16, p. 1508–1537, doi:10.1130/GES02244.1.
- EDMONDS, D.A., AND SLINGERLAND, R.L., 2007, Mechanics of river mouth bar formation: implications for the morphodynamics of delta distributary networks: *Journal of Geophysical Research*, v. 112, no. F02034, doi:10.1029/2006JF000574.
- EDWARDS, M.B., ERIKSSON, K.A., AND KIER, R.S., 1983, Paleochannel geometry and flow patterns determined from exhumed Permian point bars in north-central Texas: *Journal of Sedimentary Petrology*, v. 53, p. 1261–1270, doi:10.1306/212F835A-2B24-11D7-8648000102C1865D.
- EHLMANN, B.L., MUSTARD, J.F., MURCHIE, S.L., BIBRING, J.-P., MEUNIER, A., FRAEMAN, A.A., AND LANGEVIN, Y., 2011, Subsurface water and clay mineral formation during the early history of Mars: *Nature*, v. 479, p. 53–60, doi:10.1038/nature10582.
- FARLEY, K.A., ET AL., 2014, In situ radiometric and exposure age dating of the Martian surface: *Science*, v. 343, no. 1247166, doi:10.1126/science.1247166.
- FASSETT, C.I., AND HEAD, J.W., 2008, Valley network-fed, open-basin lakes on Mars: distribution and implications for Noachian surface and subsurface hydrology: *Icarus*, v. 198, p. 37–56, doi:10.1016/j.icarus.2008.06.016.
- FIELDING, C.R., 2006, Upper flow regime sheets, lenses and scour fills: extending the range of architectural elements for fluvial sediment bodies: *Sedimentary Geology*, v. 190, p. 227–240, doi:10.1016/j.sedgeo.2006.05.009.
- FRIEND, P.F., SLATER, M.J., AND WILLIAMS, R.C., 1979, Vertical and lateral building of river sandstone bodies, Ebro Basin, Spain: *Geological Society of London, Journal*, v. 136, p. 39–46, doi:10.1144/gsjgs.136.1.0039.
- GALLOWAY, W.E., 1989, Genetic stratigraphic sequences in basin analysis I: architecture and genesis of flooding-surface bounded depositional units: *American Association of Petroleum Geologists, Bulletin*, v. 73, p. 125–142, doi:10.1306/703C9AF5-1707-11D7-8645000102C1865D.
- GAYLORD, D.R., RITTENOUR, T.M., LINK, P.K., TURRIN, B.D., AND KUNTZ, M.A., 2021, Ghost-dune hollows of the eastern Snake River Plain, Idaho: their genesis, evolution, and relevance to Martian ghost-dune pits: *Geology*, v. 49, p. 899–904, doi:10.1130/G48645.1.
- GOUDGE, T.A., MILLIKEN, R.E., HEAD, J.W., MUSTARD, J.F., AND FASSETT, C.I., 2017, Sedimentological evidence for a deltaic origin of the western fan deposit in Jezero crater, Mars and implications for future exploration: *Earth and Planetary Science Letters*, v. 458, p. 357–365, doi:10.1016/j.epsl.2016.10.056.
- GOUDGE, T.A., MOHRIG, D., CARDENAS, B.T., HUGHES, C.M., AND FASSETT, C.I., 2018, Stratigraphy and paleohydrology of delta channel deposits, Jezero crater, Mars: *Icarus*, v. 301, p. 58–75, doi:10.1016/j.icarus.2017.09.034.
- GROTZINGER, J.P., AND MILLIKEN, R.E., eds., 2012, *Sedimentary Geology of Mars: SEPM, Special Publication 102*, doi:10.2110/pec.12.102.
- GROTZINGER, J.P., ET AL., 2014, A habitable fluvio-lacustrine environment at Yellowknife Bay, Gale Crater, Mars: *Science*, v. 343, no. 1242777, doi:10.1126/science.1242777.
- GROTZINGER, J.P., GUPTA, S., AND MALIN, M.C., ET AL., 2015, Deposition, exhumation, and paleoclimate of an ancient lake deposit, Gale crater, Mars: *Science*, v. 350, no. aac7575, doi:10.1126/science.aac7575.
- GULICK, V.C., 2001, Origin of the valley networks on Mars: a hydrological perspective: *Geomorphology*, v. 37, p. 241–268, doi:10.1016/S0169-555X(00)00086-6.
- HAGSTROM, C.A., HUBBARD, S.M., LECKIE, D.A., AND DURKIN, P.R., 2019, The effects of accretion-package geometry on lithofacies distribution in point-bar deposits: *Journal of Sedimentary Research*, v. 89, p. 381–398, doi:10.2110/jsr.2019.23.
- HAJEK, E.A., HELLER, P.L., AND SHEETS, B.A., 2010, Significance of channel-belt clustering in alluvial basins: *Geology*, v. 38, p. 535–538, doi:10.1130/G30783.1.
- HARTLEY, A.J., WEISSMANN, G.S., NICHOLS, G.J., AND WARWICK, G.L., 2010, Large distributive fluvial systems: characteristics, distribution, and controls on development: *Journal of Sedimentary Research*, v. 80, p. 167–183, doi:10.2110/jsr.2010.016.
- HAYDEN, A.T., AND LAMB, M.P., 2020, Fluvial sinuous ridges of the Morrison Formation, USA: meandering, scarp retreat, and implications for Mars: *Journal of Geophysical Research, Planets*, v. 125, no. e2020JE006470, doi:10.1029/2020JE006470.
- HAYDEN, A.T., LAMB, M.P., FISCHER, W.W., EWING, R.C., McELROY, B.J., AND WILLIAMS, R.M.E., 2019, Formation of sinuous ridges by inversion of river-channel belts in Utah,

- USA, with implications for Mars: *Icarus*, v. 332, p. 92–110, doi:10.1016/j.icarus.2019.04.019.
- HAYDEN, A.T., LAMB, M.P., AND CARNEY, A.J., 2021, Similar curvature-to-width ratios for channels and channel belts: implications for paleo-hydraulics of fluvial ridges on Mars: *Geology*, v. 49, p. 837–841, doi:10.1130/G48370.1.
- HORTON, B.K., AND DECELLES, P.G., 2001, Modern and ancient fluvial megafans in the foreland basin system of the central Andes, southern Bolivia: implications for drainage network evolution in fold–thrust belts: *Basin Research*, v. 13, p. 43–63, doi:10.1046/j.1365-2117.2001.00137.x.
- HORVATH, D.G., AND ANDREWS-HANNA, J.C., 2021, The hydrology and climate of Mars during the sedimentary infilling of Gale crater: *Earth and Planetary Science Letters*, v. 568, no. 117032, doi:10.1016/j.epsl.2021.117032.
- HUGHES, C.M., CARDENAS, B.T., GOUDGE, T.A., AND MOHRIG, D., 2019, Deltaic deposits indicative of a paleo-coastline at Aeolis Dorsa, Mars: *Icarus*, v. 317, p. 442–453, doi:10.1016/j.icarus.2018.08.009.
- HUNTER, R.E., 1977, Basic types of stratification in small eolian dunes: *Sedimentology*, v. 24, p. 361–387, doi:10.1111/j.1365-3091.1977.tb00128.x.
- IELPI, A., AND LAPÔTRE, M.G.A., 2020, A tenfold slowdown in river meander migration driven by plant life: *Nature Geoscience*, v. 13, p. 82–86, doi:10.1038/s41561-019-0491-7.
- IKEDA, S., AND PARKER, G., eds., 1989, *River Meandering*: American Geophysical Union, Water Resources Monograph 12, 485 p.
- IRWIN, R.P., CRADDOCK, R.A., AND HOWARD, A.D., 2005, Interior channels in Martian valley networks: discharge and runoff production: *Geology*, v. 33, p. 489–492, doi:10.1130/G21333.1.
- IRWIN, R.P., LEWIS, K.W., HOWARD, A.D., AND GRANT, J.A., 2015, Paleohydrology of Eberswalde crater, Mars: *Geomorphology*, v. 240, p. 83–101, doi:10.1016/j.geomorph.2014.10.012.
- JACOBSEN, R.E., AND BURR, D.M., 2018, Errors in Martian paleodischarges skew interpretations of hydrologic history: case study of the Aeolis Dorsa, Mars, with insights from the Quinn River, NV: *Icarus*, v. 302, p. 407–417, doi:10.1016/j.icarus.2017.11.014.
- JEROLMACK, D.J., AND MOHRIG, D., 2007, Conditions for branching in depositional rivers: *Geology*, v. 35, p. 463–466, doi:10.1130/G23308A.1.
- JEROLMACK, D.J., AND PAOLA, C., 2007, Complexity in a cellular model of river avulsion: *Geomorphology*, v. 91, p. 259–270, doi:10.1016/j.geomorph.2007.04.022.
- JERRAM, D.A., MOUNTNEY, N.P., HOWELL, J.A., LONG, D., AND STOLLHOFEN, H., 2000, Death of a sand sea: an active aeolian erg systematically buried by the Etendeka flood basalts of NW Namibia: *Geological Society of London, Journal*, v. 157, p. 513–516, doi:10.1144/jgs.157.3.513.
- KIM, W., PAOLA, C., SWENSON, J.B., AND VOLLER, V.R., 2006, Shoreline response to autogenic processes of sediment storage and release in the fluvial system: *Journal of Geophysical Research, Earth Surface*, v. 111, doi:10.1029/2006JF000470.
- KITE, E.S., HOWARD, A.D., LUCAS, A., AND LEWIS, K.W., 2015, Resolving the era of river-forming climates on Mars using stratigraphic logs of river-deposit dimensions: *Earth and Planetary Science Letters*, v. 420, p. 55–65, doi:10.1016/j.epsl.2015.03.019.
- KITE, E.S., MAYER, D.P., WILSON, S.A., DAVIS, J.M., LUCAS, A.S., AND DE QUAY, G.S., 2019, Persistence of intense, climate-driven runoff late in Mars history: *Science Advances*, v. 5, no. eaav7710, doi:10.1126/sciadv.aav7710.
- KOCUREK, G., ET AL., 2019, Antecedent aeolian dune topographic control on carbonate and evaporite facies: Middle Jurassic Todilto Member, Wanakah Formation, Ghost Ranch, New Mexico, USA: *Sedimentology*, v. 66, p. 808–837, doi:10.1111/sed.12518.
- KOSTASCHUK, R.A., AND VENDITTI, J.G., 2019, Why do large, deep rivers have low-angle dune beds? *Geology*, v. 47, p. 919–922, doi:10.1130/G46460.1.
- LANCASTER, N., 1988, The development of large aeolian bedforms: *Sedimentary Geology*, v. 55, p. 69–89, doi:10.1016/0037-0738(88)90090-5.
- MALIN, M.C., RAVINE, M.A., AND CAPLINGER, M.A., ET AL., 2017, The Mars Science Laboratory (MSL) mast cameras and descent imager: investigation and instrument descriptions: *Earth and Space Science*, v. 4, p. 506–539, doi:10.1002/2016EA000252.
- MALVAR, H.S., HE, L., AND CUTLER, R., 2004, High-quality linear interpolation for demosaicing of Bayer-patterned color images, *IEEE International Conference on Acoustics, Speech, and Signal Processing*, v. 3, p. iii–485, doi:10.1109/ICASSP.2004.1326587.
- MANGOLD, N., GUPTA, S., AND GASNAULT, O., ET AL., 2021, Perseverance rover reveals an ancient delta-lake system and flood deposits at Jezero crater, Mars: *Science*, v. 374, p. 711–717, doi:10.1126/science.abc4051.
- MASON, J., AND MOHRIG, D., 2018, Using time-lapse lidar to quantify river bend evolution on the meandering coastal Trinity River, Texas, USA: *Journal of Geophysical Research, Earth Surface*, v. 123, p. 1133–1144, doi:10.1029/2017JF004492.
- MASON, J., AND MOHRIG, D., 2019a, Differential bank migration and the maintenance of channel width in meandering river bends: *Geology*, v. 47, p. 1136–1140, doi:10.1130/G46651.1.
- MASON, J., AND MOHRIG, D., 2019b, Scroll bars are inner bank levees along meandering river bends: *Earth Surface Processes and Landforms*, v. 44, p. 2649–2659, doi:10.1002/esp.4690.
- MIALL, A.D., 1977, A review of the braided-river depositional environment: *Earth-Science Reviews*, v. 13, p. 1–62, doi:10.1016/0012-8252(77)90055-1.
- MILLIKEN, R.E., GROTZINGER, J.P., AND THOMSON, B.J., 2010, Paleoclimate of Mars as captured by the stratigraphic record in Gale Crater: *Geophysical Research Letters*, v. 37, doi:10.1029/2009GL041870.
- MOHRIG, D., HELLER, P.L., PAOLA, C., AND LYONS, W.J., 2000, Interpreting avulsion process from ancient alluvial sequences: Guadalope–Matarranya system (northern Spain) and Wasatch Formation (western Colorado): *Geological Society of America, Bulletin*, v. 112, p. 1787–1803, doi:10.1130/0016-7606(2000)112<1787:IAPFAA>2.0.CO;2.
- NEAL, A., RICHARDS, J., AND PYE, K., 2003, Sedimentology of coarse-clastic beach-ridge deposits, Essex, southeast England: *Sedimentary Geology*, v. 162, p. 167–198, doi:10.1016/S0037-0738(03)00136-2.
- NIELD, J.M., AND BAAS, A.C.W., 2008, Investigating parabolic and nebkha dune formation using a cellular automaton modelling approach: *Earth Surface Processes and Landforms*, v. 33, p. 724–740, doi:10.1002/esp.1571.
- OWEN, A., NICHOLS, G.J., HARTLEY, A.J., WEISSMANN, G.S., AND SCUDERI, L.A., 2015, Quantification of a distributive fluvial system: the Salt Wash DFS of the Morrison Formation, SW U.S.A.: *Journal of Sedimentary Research*, v. 85, p. 544–561, doi:10.2110/jsr.2015.35.
- PAIN, C.F., CLARKE, J.D.A., AND THOMAS, M., 2007, Inversion of relief on Mars: *Icarus*, v. 190, p. 478–491, doi:10.1016/j.icarus.2007.03.017.
- PONDRELLI, M., ROSSI, A.P., MARINANGELI, L., HAUBER, E., GWINNER, K., BALIVA, A., AND DI LORENZO, S., 2008, Evolution and depositional environments of the Eberswalde fan delta, Mars: *Icarus*, v. 197, p. 429–451, doi:10.1016/j.icarus.2008.05.018.
- PORBESKI, S.J., AND STEEL, R.J., 2006, Deltas and sea-level change: *Journal of Sedimentary Research*, v. 76, p. 390–403, doi:10.2110/jsr.2006.034.
- QUINN, D.P., AND EHLMANN, B.L., 2019, A PCA-based framework for determining remotely sensed geological surface orientations and their statistical quality: *Earth and Space Science*, v. 6, p. 1378–1408, doi:10.1029/2018EA000416.
- REITZ, M.D., JEROLMACK, D.J., EWING, R.C., AND MARTIN, R.L., 2010, Barchan-parabolic dune pattern transition from vegetation stability threshold: *Geophysical Research Letters*, v. 37, doi:10.1029/2010GL044957.
- REITZ, M.D., PICKERING, J.L., GOODBRED, S.L., PAOLA, C., STECKLER, M.S., SEEBER, L., AND AKHTER, S.H., 2015, Effects of tectonic deformation and sea level on river path selection: theory and application to the Ganges–Brahmaputra–Meghna River delta: tectonics and river path selection: *Journal of Geophysical Research, Earth Surface*, v. 120, p. 671–689, doi:10.1002/2014JF003202.
- RUBIN, D.M., LAPÔTRE, M.A.G., STEVENS, A.W., LAMB, M.P., FEDO, C.M., GROTZINGER, J.P., GUPTA, S., STACK, K.M., VASAVADA, A.R., BANHAM, S.G., BRYK, A.B., CHRISTIAN, J.R., AND EDGAR, L.A., 2022, Ancient winds, waves, and atmosphere in Gale crater, Mars, inferred from sedimentary structures and wave modeling: *Journal of Geophysical Research, Planets*, v. 127, no. e2021JE007162, doi:10.1029/2021JE007162.
- SAHOO, H., GANI, M.R., GANI, N.D., HAMPSON, G.J., HOWELL, J.A., STORMS, J.E.A., MARTINIUS, A.W., AND BUCKLEY, S.J., 2020, Predictable patterns in stacking and distribution of channelized fluvial sand bodies linked to channel mobility and avulsion processes: *Geology*, v. 48, p. 903–907, doi:10.1130/G47236.1.
- SCHOMACKER, E.R., KIEMPERUD, A.V., NYSTUEN, J.P., AND JAHREN, J.S., 2010, Recognition and significance of sharp-based mouth-bar deposits in the Eocene Green River Formation, Uinta Basin, Utah: *Sedimentology*, v. 57, p. 1069–1087, doi:10.1111/j.1365-3091.2009.01136.x.
- SEEGER, C., GROTZINGER, J.P., THOMPSON, L.M., AND KAH, L.C., 2021, Unpacking diagenetic overprints associated with the clay-sulfate transition in Gale crater, Mars [Abstract]: *Geological Society of America, Abstracts with Programs*, v. 53, no. 6, 2021, doi:10.1130/abs/2021AM-370244.
- SMITH, D.E., ZUBER, M.T., AND FREY, H.V., ET AL., 2001, Mars Orbiter Laser Altimeter: experience summary after the first year of global mapping of Mars: *Journal of Geophysical Research, Planets*, v. 106, p. 23,689–23,722, doi:10.1029/2000JE001364.
- STACK, K.M., GROTZINGER, J.P., LAMB, M.P., GUPTA, S., RUBIN, D.M., KAH, L.C., EDGAR, L.A., FEY, D.M., HUROWITZ, J.A., MCBRIDE, M., RIVERA-HERNÁNDEZ, F., SUMNER, D.Y., VAN BEEK, J.K., WILLIAMS, R.M.E., AND YINGST, R.A., 2019, Evidence for plunging river plume deposits in the Pahrump Hills member of the Murray formation, Gale crater, Mars: *Sedimentology*, v. 66, p. 1768–1802, doi:10.1111/sed.12558.
- STACK, K.M., DIETRICH, W.E., LAMB, M.P., SULLIVAN, R.J., CHRISTIAN, J.R., O'CONNELL-COOPER, C.D., SNEED, J.W., BAKER, M., ARVIDSON, R.E., FEDO, C.M., KHAN, S., WILLIAMS, R.M.E., BENNETT, K.A., BRYK, A.B., COFIELD, S., DAY, M., EDGAR, L.A., FOX, V.K., FRAEMAN, A.A., HOUSE, C.H., RUBIN, D.M., SUN, V.Z., AND VAN BEEK, J.K., 2022, Orbital and in-situ investigation of periodic bedrock ridges in Glen Torridon, Gale Crater, Mars: *Journal of Geophysical Research, Planets*, v. 127, no. e2022JE007293.
- STEIN, N., GROTZINGER, J.P., AND SCHIEBER, J., ET AL., 2018, Desiccation cracks provide evidence of lake drying on Mars, Sutton Island member, Murray formation, Gale Crater: *Geology*, v. 46, p. 515–518, doi:10.1130/G40005.1.
- STEIN, N.T., QUINN, D.P., GROTZINGER, J.P., FEDO, C., EHLMANN, B.L., STACK, K.M., EDGAR, L.A., FRAEMAN, A.A., AND DEEN, R., 2020, Regional structural orientation of the Mount Sharp Group revealed by in situ dip measurements and stratigraphic correlations on the Vera Rubin Ridge: *Journal of Geophysical Research: Planets*, v. 125, doi:10.1029/2019JE006298.
- STRAUB, K.M., PAOLA, C., MOHRIG, D., WOLINSKY, M.A., AND GEORGE, T., 2009, Compensational stacking of channelized sedimentary deposits: *Journal of Sedimentary Research*, v. 79, p. 673–688, doi:10.2110/jsr.2009.070.

- SZABÓ, T., DOMOKOS, G., GROTZINGER, J.P., AND JEROLMACK, D.J., 2015, Reconstructing the transport history of pebbles on Mars: *Nature Communications*, v. 6, no. 8366, doi:10.1038/ncomms9366.
- TEBOLT, M., AND GOUDGE, T.A., 2022, Global investigation of martian sedimentary fan features: using stratigraphic analysis to study depositional environment: *Icarus*, v. 372, no. 114718, doi:10.1016/j.icarus.2021.114718.
- TOONEN, W.H.J., KLEINHANS, M.G., AND COHEN, K.M., 2012, Sedimentary architecture of abandoned channel fills: *Earth Surface Processes and Landforms*, v. 37, p. 459–472, doi:10.1002/esp.3189.
- TRAMPUSH, S.M., HUZURBAZAR, S., AND MCELROY, B., 2014, Empirical assessment of theory for bankfull characteristics of alluvial channels: *Water Resources Research*, v. 50, p. 9211–9220, doi:10.1002/2014WR015597.
- TREVIÑO, R.H., AND VENDEVILLE, B.C., 2008, Origin of coast-perpendicular extensional faults, western Gulf of Mexico: the relationship between an early-stage ridge and a late-stage fault: *American Association of Petroleum Geologists, Bulletin*, v. 92, p. 951–964, doi:10.1306/03250807070.
- VAN WAGONER, J.C., POSAMENTIER, H.W., MITCHUM, R.M., VAIL, P.R., SARG, J.F., LOUITT, T.S., AND HARDENBOL, J., 1988, An overview of the fundamentals of sequence stratigraphy and key definitions, in Wilgus, C.K., Hastings, B.S., Posamentier, H., Van Wagoner, J., Ross, C.A., and Kendall, C.G.St.C., eds., *Sea-Level Changes: An Integrated Approach*: SEPM, Special Publication 42, p. 109–124.
- VESPREMEANU-STROE, A., PREOTEASA, L., ZĂINESCU, F., ROTARU, S., CROITORU, L., AND TIMAR-GABOR, A., 2016, Formation of Danube delta beach ridge plains and signatures in morphology: *Quaternary International*, v. 415, p. 268–285, doi:10.1016/j.quaint.2015.12.060.
- WAICHEL, B.L., SCHERER, C.M.S., AND FRANK, H.T., 2008, Basaltic lava flows covering active aeolian dunes in the Paraná Basin in southern Brazil: features and emplacement aspects: *Journal of Volcanology and Geothermal Research*, v. 171, p. 59–72, doi:10.1016/j.jvolgeores.2007.11.004.
- WEISSMANN, G.S., HARTLEY, A.J., NICHOLS, G.J., SCUDERI, L.A., OLSON, M., BUEHLER, H., AND BANTEAH, R., 2010, Fluvial form in modern continental sedimentary basins: distributive fluvial systems: *Geology*, v. 38, p. 39–42, doi:10.1130/G30242.1.
- WIGNALL, P.B., BOND, D.P.G., GRASBY, S.E., PRUSS, S.B., AND PEAKALL, J., 2019, Controls on the formation of microbially induced sedimentary structures and biotic recovery in the Lower Triassic of Arctic Canada: *Geological Society of America, Bulletin*, v. 132, p. 918–930, doi:10.1130/B35229.1.
- WILLIAMS, G.P., 1986, River meanders and channel size: *Journal of Hydrology*, v. 88, p. 147–164, doi:10.1016/0022-1694(86)90202-7.
- WILLIAMS, R.M.E., CHIDSEY, T.C., JR., AND EBY, D.E., 2007, Exhumed paleochannels in central Utah: analogs for raised curvilinear features on Mars, in Willis, G.C., Hylland, M.D., Clark, D.L., and Chidsey, T.C., Jr., eds., *Central Utah: Diverse Geology of a Dynamic Landscape*: Utah Geological Association, Publication 36, p. 221–235.
- WILLIAMS, R.M.E., ET AL., 2013a, Martian Fluvial Conglomerates at Gale Crater: *Science*, v. 340, p. 1068–1072, doi:10.1126/science.1237317.
- WILLIAMS, R.M.E., IRWIN, R.P., BURR, D.M., HARRISON, T., AND MCCLELLAND, P., 2013b, Variability in martian sinuous ridge form: case study of Aeolis Serpens in the Aeolis Dorsa, Mars, and insight from the Mirackina paleoriver, South Australia: *Icarus*, v. 225, p. 308–324, doi:10.1016/j.icarus.2013.03.016.
- WOOD, L.J., 2006, Quantitative geomorphology of the Mars Eberswalde delta: *Geological Society of America, Bulletin*, v. 118, p. 557–566, doi:10.1130/B25822.1.
- WU, C., BHATTACHARYA, J.P., AND ULLAH, M.S., 2015, Paleohydrology and 3-D facies architecture of ancient point bars, Ferron Sandstone, Notom Delta, south-central Utah, U.S.A.: *Journal of Sedimentary Research*, v. 85, p. 399–418.
- WU, C., ULLAH, M.S., LU, J., AND BHATTACHARYA, J.P., 2016, Formation of point bars through rising and falling flood stages: evidence from bar morphology, sediment transport and bed shear stress: *Sedimentology*, v. 63, p. 1458–1473, doi:10.1111/sed.12269.
- YAKIMOVSKY, Y., AND CUNNINGHAM, R., 1978, A system for extracting three-dimensional measurements from a stereo pair of TV cameras: *Computer Graphics and Image Processing*, v. 7, p. 195–210, doi:10.1016/0146-664X(78)90112-0.
- ZHAO, F., CARDENAS, B.T., AND KIM, W., 2021, Controls of aeolian dune height on cross-strata architecture: White Sands Dune Field, New Mexico, U.S.A.: *Journal of Sedimentary Research*, v. 91, p. 495–506, doi:10.2110/jsr.2020.138.

Received 28 March 2022; accepted 2 September 2022.

## APPENDIX

### 3-D Visualization of the Outcrops

As a complement to the data presented here, a scaled 3-D mesh of the Mont Mercou and Maybole outcrops have been computed using structure-from-motion photogrammetry, we followed the method described in detail by Caravaca et al. (2020) to reconstruct the exposures and their immediate surrounding for context. The resulting models were computed from hundreds of Navcam and Mastcam images, and can be viewed in the free web based Sketchfab platform at <https://skfb.ly/6ZDzO>.